Fuel 97 (2012) 288–305

Contents lists available at SciVerse ScienceDirect

Fuel

journal homepage: www.elsevier.com/locate/fuel

A breakup model for transient Diesel fuel sprays

M.R. Turner [a,*], S.S. Sazhin [a], J.J. Healey [b], C. Crua [a], S.B. Martynov [c]

[a] Sir Harry Ricardo Laboratories, School of Computing, Engineering and Mathematics, University of Brighton, Lewes Road, Brighton BN2 4GJ, United Kingdom
[b] Department of Mathematics, Keele University, Keele, Staffs ST5 5BG, United Kingdom
[c] Department of Chemical Engineering, University College London, Torrington Place, London WC1E 7JE, United Kingdom

ARTICLE INFO

Article history:
Received 13 June 2011
Received in revised form 27 January 2012
Accepted 31 January 2012
Available online 16 February 2012

Keywords:
Diesel spray
Jet breakup length
Penetration length
Modelling
Shear layer

ABSTRACT

In this paper a breakup model for analysing the evolution of transient fuel sprays characterised by a coherent liquid core emerging from the injection nozzle, throughout the injection process, is proposed. The coherent liquid core is modelled as a liquid jet and a breakup model is formulated. The spray breakup is described using a composite model that separately addresses the disintegration of the liquid core into droplets and their further aerodynamic breakup. The jet breakup model uses the results of hydrodynamic stability theory to define the breakup length of the jet, and downstream of this point, the spray breakup process is modelled for droplets only. The composite breakup model is incorporated into the KIVA II Computational Fluid Dynamics (CFD) code and its results are compared with existing breakup models, including the classic WAVE model and a previously developed composite WAVE model (modified WAVE model) and in-house experimental observations of transient Diesel fuel sprays.

The hydrodynamic stability results used in both the jet breakup model and the WAVE droplet breakup model are also investigated. A new velocity profile is considered for these models which consists of a jet with a linear shear layer in the gas phase surrounding the liquid core to model the effect of a viscous gas on the breakup process. This velocity profile changes the driving instability mechanism of the jet from a surface tension driven instability for the currently used plug flow jet with no shear layers, to an instability driven by the thickness of the shear layer. In particular, it is shown that appreciation of the shear layer instability mechanism in the composite model allows larger droplets to be predicted at jet breakup, and gives droplet sizes which are more consistent with the experimental observations. The inclusion of the shear layer into the jet velocity profile is supported by previous experimental studies, and further extends the inviscid flow theory used in the formulation of the classic WAVE breakup model.

1. Introduction

It is well established that accurate multi-dimensional modelling of the processes within Diesel engines, and similar environments, is important for various engineering applications [1–6]. This modelling must take into account many complicated processes, such as heat and mass transfer, combustion and fluid dynamics. This typically leads to relatively simple models for each of these individual processes. These models are then combined together into a Computational Fluid Dynamics (CFD) code, such as the KIVA II code [7], which is an open-source non-commercial code, widely used as a basis for the analysis of sprays [8]. This code uses a Lagrangian particle tracking approach to spray modelling, which has been shown to be advantageous compared to the Eulerian approach [9–13].

One of the most important elements of modelling Diesel fuel injections is the accurate modelling of both jet and droplet breakup. These processes are particularly important due to the sensitivity of the droplet heating, evaporation [14] and combustion processes to the droplet position and size distribution. The liquid Diesel fuel emerging from the nozzle firstly goes through a primary breakup process, where the jet breaks up into liquid sheets, ligaments and droplets, and then in the spray far field where the fuel is dispersed in the gas phase, a secondary breakup process occurs, where large droplets breakup into smaller ones [15]. In practical applications unified models are used to model both these breakup processes [16]. In these unified models, the initial jet is assumed to consist of a continuous string of injected droplets with radii equal to that of the nozzle. These large droplets then undergo breakup due to the normal and tangential stresses on their surface [17]. In most CFD codes this process is described using either the Taylor Analogy Breakup (TAB), WAVE breakup or stochastic breakup models. In the TAB model [18], which is the default breakup model in the KIVA II code, the breakup of fuel droplets is described using an analogy with a spring–mass system, while the WAVE model

* Corresponding author. Present address: Department of Mathematics, University of Surrey, Guildford, Surrey GU2 7XH, United Kingdom.
E-mail address: m.turner@surrey.ac.uk (M.R. Turner).

0016-2361/$ - see front matter © 2012 Elsevier Ltd. All rights reserved.
doi:10.1016/j.fuel.2012.01.076

[19] uses the linear stability analysis of perturbation waves on the liquid–gas interface. These approaches and their modifications [20,21], have been widely used on fuel spray computations [8,22]. In the WAVE model it is assumed that the droplets created after breakup have a predetermined size while the TAB model takes into account the distribution of droplets by radii [6,18]. The model suggested by Gorokhovski and Saveliev [23] is based on the assumption that the breakup of parent droplets, at large Weber numbers, into secondary droplets, does not depend on the instantaneous size of the parent droplets [24]. In this process the specific mechanism of atomisation and the breakup length scale cannot be clearly defined, therefore the model uses stochastic approaches to model breakup rather than deterministic ones. This model has been further developed in [25–28] (also see the recent review [29]).

A simplified spray penetration model, taking into account the effects of turbulence was suggested by Pozorski et al. [30], while the effects of droplet breakup, described by the WAVE model, on the initial stages of penetration were discussed by Sazhin et al. [31,32].

Using the unified breakup models to predict the spray penetration of Diesel fuel sprays, leads to results where the model, under–predicts penetration by around 30–50% at early times [6,33,34]. Sazhin et al. [6] attributed this difference to the neglected transient effects of the jet from the current models, which only model the jet in a quasi-steady manner. These unsteady effects are included in Sazhin et al. [6] through an *ad hoc* process where one of the model constants is reconstructed as a function of time and the newly defined constants in this function are adjusted to fit the penetration results to the experimental data. While this approach gives more accurate penetration length agreement with the experiments, the inclusion of the acceleration effects needs to be more rigorously justified and, in particular, the values of the newly defined constants need to be related to physical features of the flow. Turner et al. [35] found that for planar liquid jets, the magnitude of the acceleration seen in Diesel jet experiments is only expected to increase the breakup length of a fully unsteady jet by approximately 5%, when compared to a jet which is assumed to be quasi-steady. If a similar result holds for axisymmetric jets, which it is believed to, then this suggests that the observed difference between the CFD simulations and the experiments is unlikely to be attributed to the neglected transient effects alone.

One important feature neglected by many CFD models, is the contribution of the coherent liquid core emerging from the nozzle on the penetration length of the spray. The detailed structure within the dense spray region is not yet fully understood, and one widely referred to structure of the dense spray region is that it includes an intact liquid core and a multiphase mixing layer surrounding the core [15]. In this paper we model the intact liquid core, which is made up of a jet, ligaments and connected blobs of fuel, as a jet for simplicity, to determine whether or not this approach will improve the comparison with the Diesel jet experiments. The effect of this liquid core was included in the transient calculations of Sazhin et al. [6], by assuming that the core moves as a solid body until its diameter is halved, compared with the diameter of the nozzle. The motivation for considering this liquid core, and modelling this region as a jet, comes from Sakaguchi et al. [36] who showed, using a micro-probe Laser 2–Focus velocimeter, that the core of the spray has a heterogeneous structure throughout the steady part of the injection. It was shown that the mean axial velocity remains practically constant at downstream positions for most injection times, with these velocity values decreasing very slowly downstream in the spray.

The work of Crua et al. [37] shows, using high speed photography, a coherent liquid Diesel jet emerging from the nozzle, with small droplets being stripped from the edge of the jet, which ultimately runs into the liquid core of the spray. This agrees with the experiments of Yule and Filipovic [38], who calculate the breakup length of Diesel jets, as well as those of Badock et al. [39]. Yule and Filipovic [38] have measured the penetration length of the coherent intact liquid core into the spray, by using a cross-wind to blow the spray droplets out of the way, revealing the core. They claim that this is a coherent jet, but the subsequent work of Smallwood et al. [40] showed that conductivity probe measurements can infer a coherent jet even when the core really consists of ligaments and very dense arrays of droplets.

Following Yi and Reitz [11], the jet model approach described in the current paper uses wave packet linear stability analysis to define a jet breakup length from which we inject droplets and run droplet breakup calculations, using one of the current spray breakup models, producing spray penetration results that agree well with in house experiments at the University of Brighton facilities. In contrast to [11] our model takes into account the transient nature of the jet.

We also investigate the effect of a liquid–gas viscous shear layer on the onset of instabilities in the jet, by performing the linear stability analysis of a velocity profile with a finite thickness shear layer in the gas phase. The review paper by Lin and Reitz [41] notes that this development is important in understanding jet breakup by making the velocity profile more realistic compared with the currently used plug flow velocity profile [19].

The paper is laid out as follows. In Section 2 we discuss the current spray breakup models in more depth before formulating the proposed jet breakup model in Section 3. Section 4 gives details of the experimental data which will be used to validate our model, with the results of this validation given in Section 5. Linear stability analysis of a jet velocity profile with a viscous gas phase is examined in Section 6. The results of this analysis and the analysis of how this profile improves the composite breakup model are discussed in Section 7. Our concluding remarks and discussions are given in Section 8.

2. Spray breakup models

To describe the dynamics of liquid sprays in CFD simulations, spray breakup models, which model the breakup of droplets, are used to model the process of atomisation in a Lagrangian approach. This atomisation process is complex, and depends upon features such as the injection velocity, turbulence and cavitation effects. However, it is generally accepted that this breakup process is driven by aerodynamic stripping of smaller droplets from larger droplets (Kelvin–Helmholtz instability) or disintegration of larger droplets into smaller ones due to the effect of normal stresses (Rayleigh–Taylor instability). In Diesel sprays, these effects have been incorporated into CFD simulations using various approaches (see Stiesch [10] for a detailed review). In this paper we focus mainly on the WAVE model approach, although we also discuss the TAB and stochastic approaches as these models also has a place in CFD modelling. Below we briefly summarise these three models as well as the modified WAVE model of Sazhin et al. [6]. The reader is referred to the cited texts from each section for more information.

2.1. The classic WAVE model

The WAVE breakup model was originally developed by Reitz [19] and is based upon the temporal stability analysis of the Kelvin–Helmholtz instability for a liquid jet (density ρ_1) with an inviscid outer gas phase (density ρ_2). The velocity profile for this jet is given in Fig. 1. This Kelvin–Helmholtz instability causes 'child' droplets to be stripped from the liquid core of the jet, which is

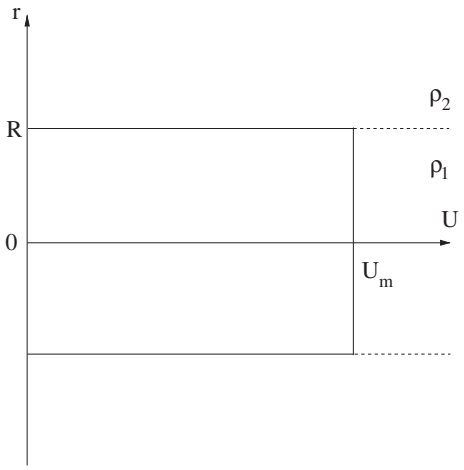

Fig. 1. Plot of the axial velocity profile $U(r)$ used in the classic WAVE model. This profile assumes an inviscid gas phase outside of the jet, and hence the profile has a discontinuity in velocity at the fluid interface $r = R$.

approximated by 'parent' droplets which have the same radius, R, as the injecting nozzle. The main problem with this approach is addressed in Section 6 where we examine a modification of the velocity profile in Fig. 1 which makes the jet more realistic, by incorporating a viscous gas phase.

The radius of the injected droplets, r_d, is assumed to continuously decrease in size during the breakup process, as described by the equation

$$\frac{dr_d}{dt} = -\frac{r_d - r_s}{\tau_{\text{bu}}}, \tag{2.1}$$

where τ_{bu} is the characteristic breakup time of the droplet, and r_s is the radius of stable droplets, given by a temporal stability analysis for the velocity profile in Fig. 1. The value of r_s is given by

$$r_s = \begin{cases} B_0\Lambda & B_0\Lambda \leqslant r_d, \\ \min\begin{pmatrix} (3\pi r_d^2 U_m/2\Omega)^{0.33} \\ (3r_d^2\Lambda/4)^{0.33} \end{pmatrix} & B_0\Lambda > r_d, \end{cases} \tag{2.2}$$

where $B_0 = 0.61$ is the model constant and Λ and Ω are the wavelength and growth rate of the fastest growing wave on the surface of the liquid jet. An approximation of these quantities for $q = \rho_2/\rho_1 \lesssim 1/10$ are given by the expressions

$$\Lambda = 9.02R\frac{(1+0.45Z^{1/2})(1+0.4T^{7/10})}{(1+0.87\text{We}_2^{5/3})^{3/5}}, \tag{2.3}$$

$$\Omega = \left(\frac{\sigma}{\rho_1 R^3}\right)^{1/2}\frac{(0.34+0.38\text{We}_2^{3/2})}{(1+Z)(1+1.4T^{3/5})}, \tag{2.4}$$

where $Z = \text{We}_1^{1/2}/\text{Re}_1$, $T = Z\text{We}_2^{1/2}$ and $\text{We}_{1,2} = \rho_{1,2}U_m^2 R/\sigma$ are the corresponding liquid and gas Weber numbers respectively [19]. The quantity $\text{Re}_1 = U_m R/\nu_1$ is the liquid Reynolds number. The breakup time, τ_{bu}, is given by

$$\tau_{\text{bu}} = 3.7626\frac{B_1 R}{\Lambda\Omega}, \tag{2.5}$$

where B_1 is an adjustable model constant which varies approximately between $\sqrt{3}$ and 20 [8,19] depending upon the type of injector being used. Eq. (2.1) with τ_{bu} defined by (2.5) has been shown to be consistent with the experiments of Reinecke and Waldman [42].

This model was extended by Patterson and Reitz [20] who incorporated the Rayleigh–Taylor instability of droplets, which mainly accounts for the secondary breakup of droplets, while the stripping Kelvin–Helmholtz instability mainly accounts for the primary breakup process [21]. This model was modified to incorporate transient effects by Sazhin et al. [6], see Section 2.4. The classic WAVE model will be the main droplet breakup model used in our composite breakup model in Sections 5 and 7.

2.2. The TAB model

The Taylor Analogy Breakup (TAB) model is the default breakup model used in the KIVA II code, and it describes the droplet breakup process in terms of the critical deformation of the oscillating droplet [18]. The normalised radial droplet deformation is given by $y = 2e/r_d$, where e is the extension of the droplet radius from its equilibrium position and r_d is the droplet radius. The time evolution of this quantity is described by the forced, damped linear harmonic oscillator

$$\frac{d^2y}{dt^2} = \frac{2\rho_2 U_m^2}{3\rho_1 r_d^2} - \frac{8\sigma}{\rho_1 r_d^3}y - \frac{5\mu_1}{\rho_1 r_d^2}\frac{dy}{dt}, \tag{2.6}$$

where the external forcing comes from the relative motion of the drop, the restoring force is surface tension and the damping force is the fluid dynamic viscosity, μ_1. The solution for $y(t)$ can be found analytically, and breakup is modelled by assuming that $y = 1$ at the moment of breakup.

The Sauter Mean Radius (SMR), S, of the droplets at the moment directly after breakup can be found from the conservation of droplet energy during breakup

$$S = \frac{r_p}{\frac{7}{3} + \rho_1 r_p^3\left(\frac{dy}{dt}\right)_{\text{bu}}^2/8\sigma},$$

where r_p is the radius of the parent droplet and $(dy/dt)_{\text{bu}}$ is the value of dy/dt at breakup, i.e. when $y = 1$. Unlike the WAVE model, the TAB model produces a distribution of droplet sizes after breakup, given by

$$f(r_d) = \frac{3}{S}\exp\left(-\frac{3r_d}{S}\right). \tag{2.7}$$

The results predicted by the TAB model in O'Rourke and Amsden [18], for modelling fuel sprays, agree well with the experimental results of Hiroyasu and Kadota [43]. This model, however, over-predicts the rate of breakup and tends to under-predict the droplet size close to the injector. It was modified by Tanner [44] to enable it to describe breakup at larger Weber numbers, which is the dominating mechanism in the primary breakup region of liquid jets.

2.3. The stochastic model

The WAVE model described in Section 2.1 is essentially a deterministic model where the radii of the droplets formed at breakup are determined by (2.1). The TAB model in Section 2.2 contains a stochastic element by assuming that the sizes of the product droplets are given by the predetermined distribution (2.7). The approach laid out in Gorokhovski and Saveliev [23] is different to the two previous methods because it is focused on the analysis of the time evolution of the distribution of droplets by radii. It assumes that the breakup of a parent droplet into secondary droplets does not depend upon the size of the parent droplet at breakup (Kolmogorov hypothesis [24]). This approach is appealing in high pressure injection sprays where the Weber number is large, and breakup is due to the Kelvin–Helmholtz instability, but turbulent fluctuations in the problem make the specific breakup mechanism and the scale of the breakup hard to define.

Gorokhovski and Saveliev [23] showed that in the large time limit, $t \to \infty$, the equation for the droplet number distribution function for parent droplets, $F(r_d)$, which gives $F(r_d)dr_d$ droplets in

the interval dr_d, can be represented by a Fokker–Planck type equation

$$\frac{\partial F}{\partial t} = \left(-3\langle \ln \xi\rangle - \frac{9}{2}\langle \ln^2 \xi\rangle - \frac{\partial}{\partial r_d} r_d \langle \ln \xi\rangle + \frac{1}{2}\frac{\partial}{\partial r_d} r_d \frac{\partial}{\partial r_d} r_d \langle \ln^2 \xi\rangle\right) \nu F(r_d), \tag{2.8}$$

where

$$\langle \ln^n \xi\rangle = \int_0^1 \ln^n \xi \; \chi(\xi)\, d\xi.$$

The parameter $\xi = r_d/r_0 \in [0, 1]$ links the radius of the product droplets (r_d) to the parent droplets (r_0), $\chi(\xi)d\xi$ is the normalised probability that the radius of each product droplet is in the range $[\xi r_d, (\xi + d\xi)r_d]$ and $\nu = \nu_0\chi_0$, where ν_0 is the breakup frequency of an individual droplet and χ_0 is the average number of droplets produced after each breakup mechanism.

The two unknown constants in (2.8), $\langle \ln\xi\rangle$ and $\langle \ln^2\xi\rangle$, can be thought of as fitting parameters. In order to get an agreement with the experimental results of Hiroyasu and Kadota [43] they were taken to be $-1/2$ and 1 respectively. The frequency of the breakup ν was then estimated as

$$\nu = \frac{|U_m|}{C r_0}\sqrt{\frac{\rho_2}{\rho_1}},$$

where the constant $C = \sqrt{3}$ was chosen to match experimental data on the stripping breakup regime. Further developments of this model are discussed in [25–28]. See [29] for further details.

The three models described in Sections 2.1,2.2,2.3 have mainly been validated on sprays which are injected at either a constant or a slowly varying velocity. However, when comparing the results of these models to transient Diesel jet injection measurements, it has been found that the CFD simulations underestimate the observed spray penetration length at early times [6]. In this paper we produce results which show that the inclusion of a liquid core, that penetrates a certain distance into the spray before it begins to break up into ligaments and droplets, leads to predictions that agree well with the experiments. This approach is similar to that of Sazhin et al. [6], who modified the WAVE model to include this coherent core, as discussed in the next section, but many important details are different from those described in [6].

2.4. The modified WAVE model

The WAVE model described in Section 2.1 has been modified in [6] to account for the transient nature of the Diesel jet injection. This transient effect was incorporated by modifying the parameters from the classic WAVE model to control the rate of spray disintegration. It was assumed that an acceleration effect due to the injection process would lead to a decrease in the value of Ω, while leaving the wavelength of the critical instability Λ unchanged. The decrease in the value of Ω, with increasing acceleration was thought to mimic the observed relaminerisation of the flow and the thickening of the boundary layer in the gas phase surrounding the jet [45]. The thickening of the shear layer is expected to stabilise the fluid interface [46]. As the WAVE breakup time $\tau_{bu} \sim 1/\Omega$ the effect of the transient injection is included into the model by multiplying the model constant B_1 in (2.5) by a function of jet velocity and acceleration. It is suggested that

$$B_1^{\text{mod}} = B_1(1 + c_1(a^+)^{c_2}), \tag{2.9}$$

where

$$a^+ = 2\sqrt{\text{Re}_2}\,\frac{r_d}{U_{\text{inj}}^2}\,\frac{dU_{\text{inj}}}{dt}$$

is the acceleration parameter, c_1 and c_2 are adjustable model constants and Re_2 is the gas Reynolds number. This acceleration parameter is constructed in analogy with the local pressure gradient parameter suggested by Cebeci and Smith [47] assuming a laminar dependence of the local skin friction coefficient on the Reynolds number.

This model also incorporates a coherent liquid core along with the stabilizing of the disturbance growth. This core is incorporated into the model by assuming that droplet parcels in the liquid core do not experience any drag from the gas phase, and, as the injection velocity U_{inj} varies, then every parcel in the liquid core has their velocity instantaneously modified to equal U_{inj}. This is incorporated into KIVA II by using a modified version of the collision algorithm of Nordin [48] for droplets in the liquid core and the conventional algorithm by O'Rourke [49] away from the core. The radius of this liquid core is allowed to decrease due to stripping of droplets from its surface. This process continues until its radius becomes half the radius of the nozzle. After this, the modified WAVE model is activated.

Other models such as those of [11,50,51] use the classic WAVE breakup model from a predetermined jet breakup length to calculate spray penetration results, but this core breakup length is estimated assuming the injection velocity is constant. In the next section we formulate a jet breakup model to approximate the liquid core which can be combined with one of the spray breakup models in Sections 2.1,2.2,2.3 to generate predictions for the penetration length of transient Diesel sprays.

In this paper we assume that the explicit effect of viscosity on the breakup process is small enough, so that we can consider it as inviscid. Therefore, the effect of viscosity in the above four models is neglected, so $Z = T = 0$ in (2.3) and (2.4) and $\mu_1 = 0$ in (2.6). This assumption is justified later in the paper.

3. Jet breakup model for primary breakup

Computational Fluid Dynamics simulations using the droplet breakup models described in Sections 2.1,2.2,2.3, give good agreement with experimental observations when the spray is assumed to emanate directly from the nozzle and when the injection velocity is constant or slowly varying [18,19,23]. But for Diesel jet experiments, the agreement is less good at early injection times [6,33,34]. The experiments of Crua et al. [37] and Badock et al. [39] show that these Diesel injections have a coherent liquid jet emerging from the nozzle, at least for early injection times, and these jets do not behave as a continuous string of injected droplets as is employed currently in most spray models. In this section we model the primary breakup of these jets into droplets and incorporate this model into the KIVA II code to simulate the effect of the liquid core of the spray. A similar approach was incorporated into the KIVA II code by Sazhin et al. [6]. Their model, however, was based on the introduction of two extra model constants, with no clear physical meanings, to damp the Kelvin–Helmholtz instability by jet acceleration. These constants had to be adjusted to generate the agreement with experimental data. In the model described below we only have one undetermined constant which is related to the primary breakup time of the jet.

At early injection times the experimental results of Karimi [52] show that the injection velocity of the jet, estimated from the mass flow rate, is approximately equal to velocity of the jet tip (see Fig. 2b). This suggests that at early times the jet can be approximately modelled as a rigid cylindrical body. This assumption is supported by the experiments of Sakaguchi et al. [36] and Schugger et al. [53] who indicate that there is a conservation of momentum in the liquid core of the spray. In this case the penetration length of the solid jet, L_s, is given by

$$L_s = \int_0^t U_m(t')\, dt',$$

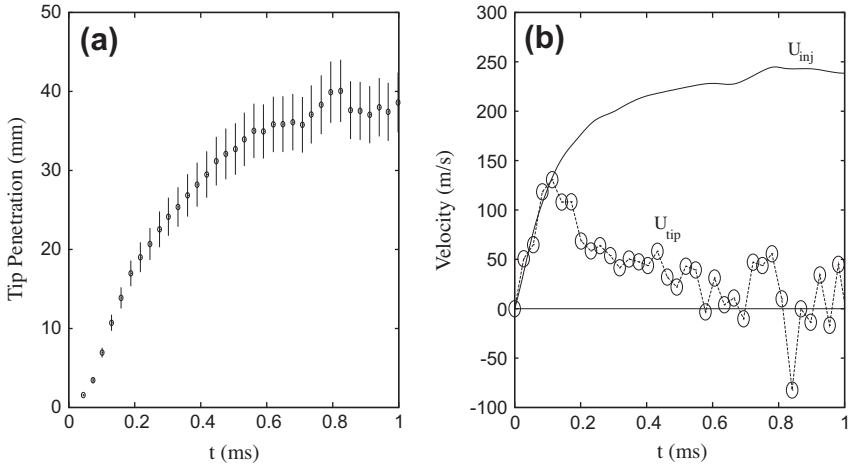

Fig. 2. Plot of (a) the experimentally observed spray penetration length for a 7-hole injector where the fuel was injected with an injection pressure p_{inj} = 60 MPa into stagnant air at a pressure p_g = 2 MPa and temperature 410 K. The temperature of the fuel was approximately 410 K and the vertical lines indicate the 20% error bars of the data. Panel (b) plots the injection and spray tip mean velocities for the same conditions.

where U_m is the jet velocity (see Fig. 1). We assume that this approximation is valid until the time when the jet first begins to break up.

Turner et al. [35] show that the breakup length of an accelerating planar jet can be well approximated by considering the integral of the group velocity of the fastest growing disturbance wave packet on the surface of the jet, from the time it is released from the nozzle, $t - \tau_b$, to the point at which it breaks up t, where τ_b is the breakup time. Here it is assumed that disturbance waves of all frequencies are generated at the nozzle due to the injection process. This is a reasonable assumption to make because there are various mechanisms in the injection process that can induce disturbances in the jet. These mechanisms include the vibration of the injector nozzle, the vibration of the injector needle, cavitation effects within the nozzle, and fuel pressure oscillations due to the high pressure pump. The assumption that disturbances of all frequencies are generated at the nozzle is widely used in the linear stability analysis of jets and wakes [54,55,35], as well as being a fundamental assumption in the WAVE breakup model in Section 2.1. The jet breakup length, L_{bu} is determined by solving

$$L_{bu} = \int_{t-\tau_b(U_m)}^{t} c_g(t')\,dt', \tag{3.1}$$

where c_g is the group velocity of the fastest growing disturbance. This equation is valid for $t - \tau_b(U_m) > 0$, and for times before this, the jet has yet to breakup. Therefore, by making this coherent jet assumption for modelling the liquid core, we are assuming that the disturbance wave propagates downstream even if the liquid core is not a coherent jet, but is made up of a highly dense spray. In agreement with the WAVE model theory in Section 2.1, we assume that the jet has a plug flow velocity profile, with an inviscid gas phase, for all injection times, as in Fig. 1. For Diesel jets, a typical value for the Weber number is $We_2 = O(10^3)$, so we can assume we are in the stripping regime for the jet breakup [19]. Therefore, c_g/U_m is solely a function of We_2, where c_g/U_m is a constant between 0.91 and 0.99 for $q = \rho_2/\rho_1$ between 1/10 and 1/100 in the large Weber number limit. In this study we assume that the breakup time for the jet τ_b is identical to that of the WAVE model, τ_{bu}, given by (2.5). In the large We_2 stripping breakup limit with $Re_1 \gg 1$,τ_b becomes

$$\tau_b = B_1' \frac{R}{U_m} q^{-1/2}, \tag{3.2}$$

by using (2.3) and (2.4), where B_1' is a model constant which should be in the same value range as B_1 in Section 2.1. This stripping breakup time was estimated by fitting curves to experimental data [19,56], and is widely used in the literature and CFD codes, such as in [18,32] for example. As τ_b is a function of the jet velocity $U_m(t)$, (3.1) cannot be solved analytically because variations in t occur in both the integrand and the upper limit of the integral, thus L_{bu} is determined numerically once $U_m(t)$ is determined from the experimental data. The breakup length of the jet, L, is then found to be

$$L = \min(L_s, L_{bu}),$$

at each time t.

This jet breakup model is incorporated into the KIVA II code to predict the penetration length of the spray when used with one of the classic droplet breakup models from Sections 2.1,2.2,2.3. This is achieved by releasing droplet parcels from the leading edge of the jet for $t > \tau_b(t)$ of radius r_s, which is the stable droplet radius generated by the jet in (2.2) with $r_d = R$ and $U_m = U_{inj}$. (Note, however, that once these droplets are released from the core their breakup characteristics are changed through (2.3)–(2.5) and so their size will continue to reduce over time and further secondary breakups of the droplet will occur.) The secondary breakup of these droplets can then be determined by using one of the classic breakup models in Sections 2.1,2.2,2.3. The WAVE model will be used in our analysis, and we make this choice because the WAVE model is a hydrodynamic stability model, as is our jet breakup model. In Section 5 we use this composite breakup model approach to analyse the experimentally observed results described in Section 4.

4. Experimental observations

In this paper we compare the results of our composite breakup model against Diesel spray experiments conducted at the University of Brighton in the Sir Harry Ricardo Laboratories. The spray visualisations were carried out using a reciprocating rapid compression machine based around a Ricardo Proteus single cylinder engine converted to liner ported, 2 stroke cycle operation [57]. The removal of the valve train allowed the fitting of an optical chamber of 80 mm in height and 50 mm diameter into the cylinder head. The optical access to the combustion chamber was provided by three removable sapphire glass windows. Due to the increased volume of the combustion chamber, the compression ratio was

reduced to 9:1. The intake air was conditioned to simulate a modern Diesel engine with a compression ratio of 19:1. For the present experiments the peak in-cylinder pressures and temperatures were intentionally kept low in order to reduce the evaporation rate and inhibit autoignition. No swirl was generated, and the air was quiescent at the time of injection.

The fuel was a low sulphur reference Diesel representative of automotive Diesel fuel. It was delivered by a 2nd generation Bosch common–rail system, comprising a high–pressure pump rated at 160 MPa. The rail pressure, timing and duration of the injection were independently controlled by a custom–built fuel injection controller.

Two injectors were used for the present study. The first was a Delphi DFI1.3 injector fitted with a 7-hole valve-closed orifice (VCO) nozzle. The nozzle orifices were cylindrical with a diameter of 0.135 mm and a length of 1 mm. This injector was extensively characterised on a macroscopic scale by high-speed video and laser diagnostics [52], and was used with an injection pressure of 60 MPa into an in-cylinder pressure of 2 MPa and temperature of 410 K ($q \approx 0.0227$). The second injector was a Bosch VCO nozzle, with a single cylindrical orifice with a diameter of 0.2 mm and a length of 1 mm. This injector was used with an injection pressure of 160 MPa into an in-cylinder pressure of 4 MPa and temperature of 580 K ($q \approx 0.0360$).

The injection velocity and the discharge coefficient were measured using the long-tube rate of injection technique, and derived from the instantaneous measurements of the rate of injection [52]. The high-speed camera used for spray visualisation featured an 8-bit monochromatic CMOS sensor, and a global electronic shutter with exposures down to 2 μs. Compromise between acquisition rate and resolution was obtained with a frame rate of 34,300 frames per second, with a corresponding maximum resolution of 128 × 320 pixels. The processing of the video frames for measurement of the spray penetration was performed by purpose-developed software [57]. Suitable thresholding was carried out in order to pick out the tip of unbroken portion of the spray outline furthest from the nozzle on the spray axis, from the background.

From the measured mass flow rate information, we estimate the injection velocity of the jet at each nozzle as

$$U_{\text{inj}} = (\rho_1 A_0 n)^{-1} \frac{dm}{dt}, \tag{4.1}$$

where A_0 is the cross-sectional area of each nozzle and n is the number of nozzles. Therefore, for the 7-hole injector, we are only considering the spray propagation from one of the seven holes. There is little experimental information showing how the velocity profile in the jet evolves in the streamwise direction, but Sakaguchi et al. [36] shows that the mean axial velocity in this direction is approximately constant, with a slow decrease at larger downstream distances. Therefore, in our model we assume that $U_m = U_{\text{inj}}$ for all times. For this 7-hole nozzle, the experimental spray penetration length, injection velocity and spray tip velocity are plotted in Fig. 2.

In the current study we assume that the liquid jet fills the nozzle completely as it injects into the cylinder, i.e. we assume no cavitation effects. This means that the injection velocity calculated from (4.1) is assumed to be the injection velocity seen in the experiment. Cavitation effects are beyond the scope of this paper, but could be incorporated into this study [22,58], and this would correspond to modifying the injection velocity by

$$U_m = U_{\text{inj}}/C_c,$$

where $C_c \leqslant 1$ is the contraction coefficient, which can reach a minimum of approximately 0.62 for super-cavitating flows [59].

For the single hole injector results, the spray penetration length and injection velocity is plotted in Fig. 3. For this injector there was initially a hesitation period in the injection (not shown) where the fluid was partially injected, and then the injection stopped, before the remaining fluid was injected without any further delay [52]. This initial hesitation period, caused by a non-axisymmetric pressure distribution on the tip of the injector's needle, gave a non-zero penetration length caused by the initial injection of fluid. The remaining fluid then injects through on the main part of the injection. In this paper we are only interested in the second injection period as this is the main injection of the fuel, hence the hesitation time period is subtracted from the results.

For both sets of experimental data plotted in Fig. 2b and Fig. 3b, cluster shedding was observed from the tip of the spray. This leads to fluctuations of the observed penetration length at around 40 mm, for both sets of data. This phenomenon has not been addressed in the present study. We also anticipate that the experimentally observed penetration length will be longer than that documented here, due to the spray extending beyond the windows of the optical rapid compression machine.

5. Results of the composite spray breakup model

In this section we compare results for the composite spray breakup model with the data for the 7-hole injector from Section

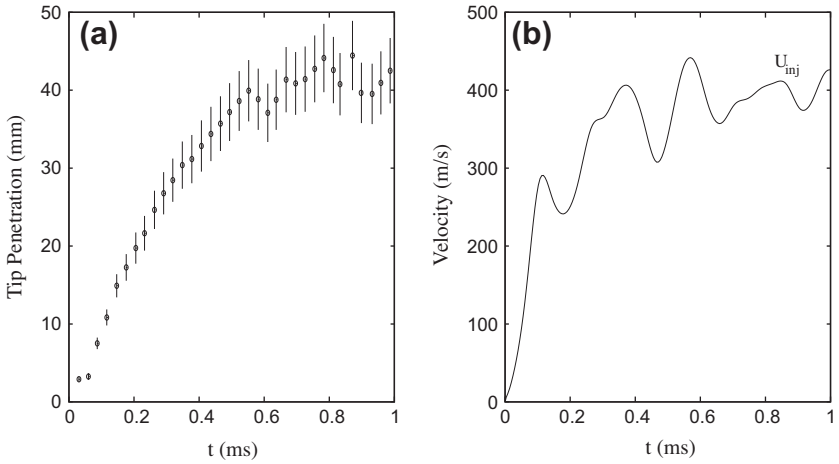

Fig. 3. Plot of (a) the experimentally observed spray penetration length for a single hole injector where the fuel was injected with an injection pressure p_{inj} = 160 MPa into stagnant air at a pressure p_g = 4 MPa and temperature 580 K. The temperature of the fuel was approximately 490 K and the vertical lines indicate the 20% error bars of the data. Panel (b) plots the mean injection velocity for the same conditions.

4. The composite model is incorporated into the KIVA II CFD code, and simulations are performed on a two-dimensional axisymmetric uniform mesh covering a closed engine cylinder domain, 20 mm in the radial direction and 100 mm in the axial direction. The boundaries of the domain are assumed to be solid walls with a no slip boundary condition imposed on them. The grid resolution used for the simulations is 40×100 (radial $\times$ axial) using 10^4 droplet parcels per 1 ms of injection time. The results for this grid resolution were checked against the finer grid resolutions 80×100 and 40×150 and are found to be grid independent to within a few percent. (Note that dependence on grid size will start to appear for very fine grids [60] using the Lagrangian approach.)

Throughout the rest of this paper, all the breakup processes are assumed to be inviscid, except in Fig. 5 where we analyse our inviscid breakup assumption. However, viscous effects are still considered in the spray model, through the droplet/gas interaction algorithm of the KIVA II code. Before we investigate the composite breakup model, we first examine the results of the three classic spray breakup models, outlined in Section 2. These results are plotted in Fig. 4a.

The results for the existing classic models show that each model under-predicts the penetration length of the spray for early injection times, in agreement with the results of the single hole injector presented in Sazhin et al. [6]. Curve 1 shows the result with no breakup model included. This result gives the penetration of droplets of a fixed radius, $r_d = R$, which slow down due to air resistance, and are advected in the gas phase due to the induced velocities in the gas phase caused by the droplet/gas interaction. We see that the other four results, which include breakup effects, have penetration lengths similar to curve 1 at very early times, before deviating from it as breakup occurs. The breakup causes the droplets to reduce in size and slow down more rapidly compared to the no breakup result. The two WAVE model results (curves 2 and 3) give the best approximations to the experimental penetration length, i.e. give the minimum error between the experimental data and the simulation at early times. Note that the circles give the upper and lower bounds for each experimental measurement. The TAB and stochastic models on the other hand, underestimate the experimental data more than the WAVE model. The maximum percentage difference between the model result and the observed data points for $t < 0.5$ ms is approximately 35–40%.

In Fig. 4b we examine the result of the modified WAVE model from Section 2.4 with $B_1 = 10$, $c_1 = 1$ and $c_2 = 0.2$. The results show that the modified WAVE model result (curve 2) gives a much better penetration length agreement with the experiment than the classic WAVE model result (curve 1). However, if we incorporate only the rigid core part (curve 3) or the effect of damped Kelvin–Helmholtz instability due to acceleration (see Eq. (2.9)) (curve 4) part of the modified WAVE model then, the agreement with the experiment is lost and both results have penetration lengths similar to the classic WAVE model result. This suggests that both parts of the modified WAVE model are needed to gain agreement with the experiment. However, the results of our composite model in the remainder of this section will show that only the inclusion of the liquid core is required to gain good agreement with the experiments.

For the remaining results in this paper we focus on the classic WAVE breakup model to model the secondary breakup of droplets in our composite breakup model. However, we do investigate composite models using the other two classic breakup models later in this section as a comparison. In Fig. 5 we show that the inviscid assumption made on the breakup models earlier in this section is valid, and the effect of viscosity in the WAVE breakup model, with $B_1 = 10$, is to increase the penetration length slightly. In this figure viscosity is included by giving the Reynolds number for the Diesel jet, Re_1, its actual value from the experimental data, rather than assuming it is infinite. Thus, the breakup properties (2.3) and (2.4) are adjusted accordingly. The observed increase in the penetration length is due to the radius of the droplets at breakup being about 20% larger than the inviscid result, as shown in the SMR results, measured at $x = 30$ mm and $r = 0$ mm, in Fig. 5b.

The effect of the coherent jet is incorporated into the KIVA II droplet model, by fixing droplets of radius $r_d = R$ in the region from $x = 0$ to $x = L(t)$. These droplets are placed a distance of $R/100$ apart and each is given the velocity U_{inj}, parallel to the jet axis. This then represents the coherent jet, which updates the gas phase velocities accordingly, via the viscous interaction with the gas phase. To make sure we have conservation of mass in our model, we take the mass of fuel injected at a time t, subtract off any fuel which remains in the coherent core (this is possible because we know $L(t)$) and the remaining mass is then assumed to be droplets which have been stripped off the coherent core.

This approximation of the coherent liquid core is cruder than that of Sazhin et al. [6] as its radius is assumed to remain constant in this study, while Sazhin et al. allowed their core radius to reduce. However, allowing this core to thin would require

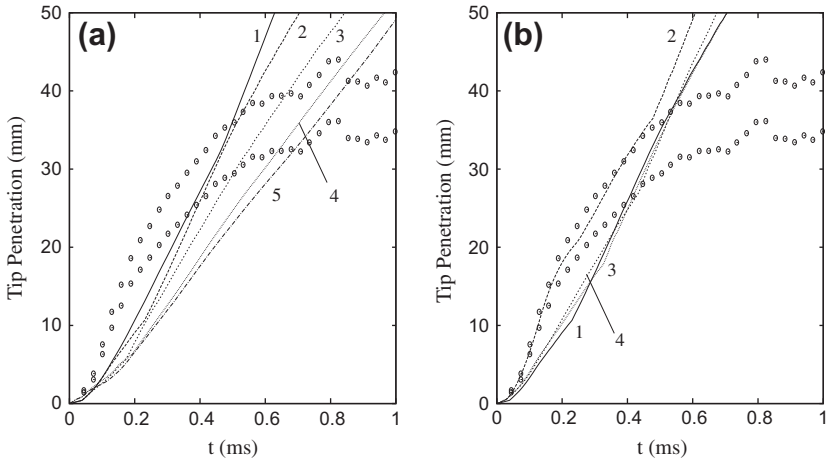

Fig. 4. Plot of (a) the spray penetration length as a function of time for the 7-hole injector using the classic breakup models of Section 2. The results correspond to 1 – no breakup model, 2 – the classic WAVE model with $B_1 = 10$, 3 – the classic WAVE model with $B_1 = 1.73$, 4 – the TAB model and 5 – the stochastic model. In each breakup model viscosity is neglected and the circles give the upper and lower limits of the error bars for the experimental observations. Panel (b) plots the penetration length for 1 – the classic WAVE model with $B_1 = 10$, 2 – the modified WAVE model, 3 – the modified WAVE model only incorporating the rigid core model and 4 – the modified WAVE model without taking into account the effect of acceleration on the rigid core. In each modified WAVE model result the model constants are $B_1 = 10$, $c_1 = 1$ and $c_2 = 0.2$.

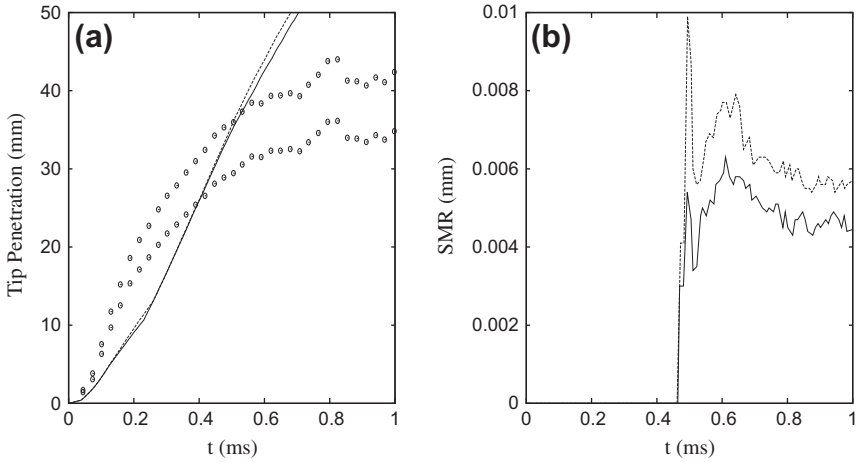

Fig. 5. Plot of the classic WAVE model result with $B_1 = 10$ from Fig. 4 (solid curve) and the corresponding result with viscosity included (dashed curve) for (a) the penetration length and (b) the SMR at $x = 30$ mm and $r = 0$ mm. The circles give the upper and lower limits of the error bars for the experimental observations.

information about how it thins both spatially and temporally, which would introduce new parameters into this model, and besides, the only difference this would make to the current model is to allow more fuel to be dispersed as droplets rather than being held within the liquid core.

In Fig. 6a we plot both the solid jet tip position, L_s, (curve 5) and the jet breakup length L_{bu} with $B_1' = 3, 4, 5$ and 6, numbered 1–4 respectively, for the jet breakup model. As the value of c_g/U_m for the plug flow jet with an inviscid air layer is close to unity for this density ratio ($q \approx 1/44$), we set it equal to one for all the results in this figure to simplify the analysis. This is acceptable at this stage as we are exploring the validity of the composite model. The results show that L_s (solid line) gives good agreement with the experimental data for $t \leqslant 0.15$ ms, which agrees with the time range where $U_{inj} = U_{tip}$ in Fig. 2. The results for L_{bu} (dashed lines) can then be seen to emerge from L_s (because we have set $c_g/U_m = 1$) at different times which depend on the value of B_1' chosen. The time at which each dashed line first appears (i.e. is separated from the solid line) in Fig. 6a is the initial breakup time of the jet, which corresponds to the time where $t = \tau_b$ in (3.1). This initial breakup time increases as the model constant B_1' is increased. The breakup length of the jet, L, is then found by taking the minimum value of L_s and L_{bu} for each time value. The results in Fig. 6a show that the breakup length of the jet follows the leading edge of the jet up to the point at which the jet initially breaks up. It then increases more slowly, and eventually levels out to a constant breakup length which is less than the penetration length of the observed spray. This leveling off of L_{bu} is due to the injection velocity U_{inj} becoming approximately constant in Fig. 2b. When we include the classic WAVE spray model of the KIVA II code to act on this breakup length, with $B_1 = B_1'$, we generate the predicted penetration lengths of the spray which are given in Fig. 6b, where again curves 1–4 show the results for $B_1' = B_1 = 3, 4, 5$ and 6 respectively. These penetration results follow the jet breakup results from Fig. 6a initially and then once the breakup length of the jet levels off, the penetration length increases at a slower rate which is similar to the rate of increase seen in the classic WAVE model results in Fig. 4a. The results in Fig. 6b show that there is a small range of B_1' values where the composite model results lie within the error bars of the experimental results. For this particular example this range is approximately $B_1' \in [4, 6]$, and the agreement is generally good for $t \lesssim 0.5$ ms.

This composite breakup model approach can also be implemented using the classical Levich breakup length formula [61] for an injecting jet at a constant velocity. This formula states that

$$L_{bu}^{Lev} = C_L R q^{-1/2},$$

where C_L is an adjustable model constant. Fig. 7a plots $L_{bu}^{Lev}(t)$ for $C_L = 4.91$ (curve 1) and 3.91 (curve 2) and Fig. 7(b) plots the

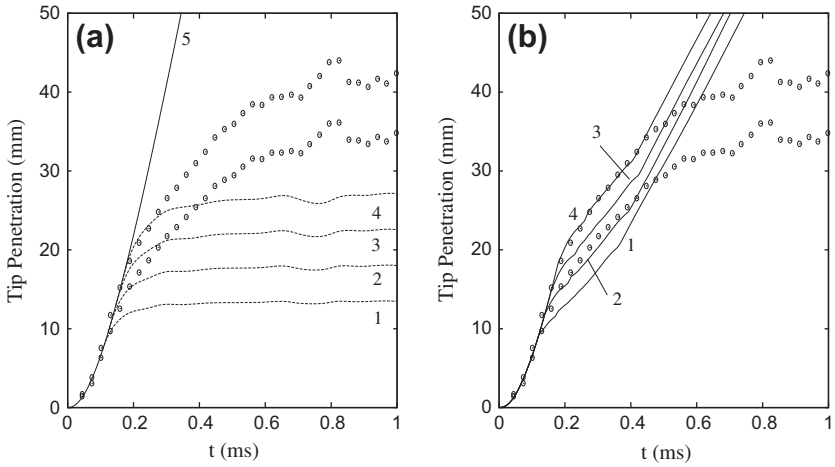

Fig. 6. Plot of (a) $L_s(t)$ (curve 5) and $L_{bu}(t)$ for the 7-hole injector with $B_1' = 3, 4, 5$ and 6 represented by curves 1–4 respectively. Panel (b) plots the penetration length predicted by the composite model with $B_1 = B_1'$ in the classic WAVE breakup model. The circles give the upper and lower limits of the error bars for the experimental observations.

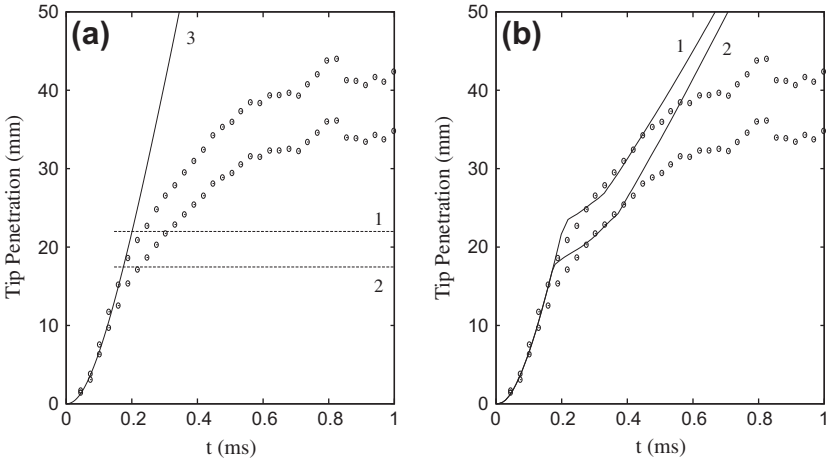

Fig. 7. Plot of (a) $L_s(t)$ (curve 3) and L_{bu}^{Lev} for the 7-hole injector with $C_L = 4.91$ (curve 1) and 3.91 (curve 2). Panel (b) plots the penetration length of the spray predicted by the composite model with $B_1 = 5$ in the classic WAVE breakup model. The circles give the upper and lower limits of the error bars for the experimental observations.

corresponding penetration length with $B_1 = 5$. The result with $C_L = 4.91$ has a jet breakup length which is approximately equal to that of the quasi-steady approach with $B_1' = 5$, and we see that the penetration length slightly over-estimates the experimental results around $t = 0.2$ ms. However, the agreement can be improved by by reducing the value of C_L, which like B_1' is nozzle dependent, to 3.91 (curve 2). While using L_{bu}^{Lev} instead of the quasi-steady L_{bu} may be acceptable in certain cases, the benefit of the quasi-steady result is that the transient behaviour of the injection is taken into account. Therefore, we recommend the use of the the quasi-steady break-up length (3.1) in numerical simulations.

In Fig. 8 we plot the breakup length and penetration results, as in Fig. 6, except for the single hole injector. This is to demonstrate that the composite model predicts accurate results for a range of different injection conditions. As for the 7-hole case, we find good agreement for the jet breakup length for $t \leqslant 0.15$ ms, but here the values of B_1' chosen to gain the agreement with the experimental data are less than in the 7-hole case, and so these results give a slightly shorter breakup length. This result agrees qualitatively with the experiments of Yule and Filipovic [38], who show that the breakup length of the liquid core decreases with both an increased value of p_{inj} and p_g. When we include the WAVE spray breakup model with these jet breakup length predictions in Fig. 8b, we again see that we get penetration results that agree well with the experiment. Here, however, the agreement is only good for $t \lesssim 0.35$ ms, which is a shorter time range than for the 7-hole injector. But this is to be expected, because at these high injection pressures (and thus velocities) we expect effects such as cavitation to be important [62]. Hence the fact that this approach gives agreement even for this small time range should be considered as encouraging.

In Fig. 9 we plot the composite model results and the modified WAVE model results for (a) the 7-hole and (b) the single hole injectors. These results show that the jet composite model produces penetration length results which agree well with the experiments and with the corresponding modified WAVE model results. In Section 7 we find that our composite model results agree even better with the experiments after we modify the model to give a spray shape that agrees better with experiments. The corresponding values of B_1^{mod} for each modified WAVE model result is plotted in panel (c). This panel shows that the modified WAVE model damps the Kelvin–Helmholtz instability, for each data set, by increasing the value of B_1^{mod} in comparison to the value of B_1. This increase remains even at later injection times, with $B_1^{mod} \approx 16$, and returns to $B_1^{mod} = 10$ when $a^+ < 0$ due to $0 < c_2 < 1$. This larger value of B_1^{mod} means the droplets reduce in size slower from (2.1), so they are larger with more momentum at later times, thus the penetration length is longer. At very early times, the value of B_1^{mod} is a

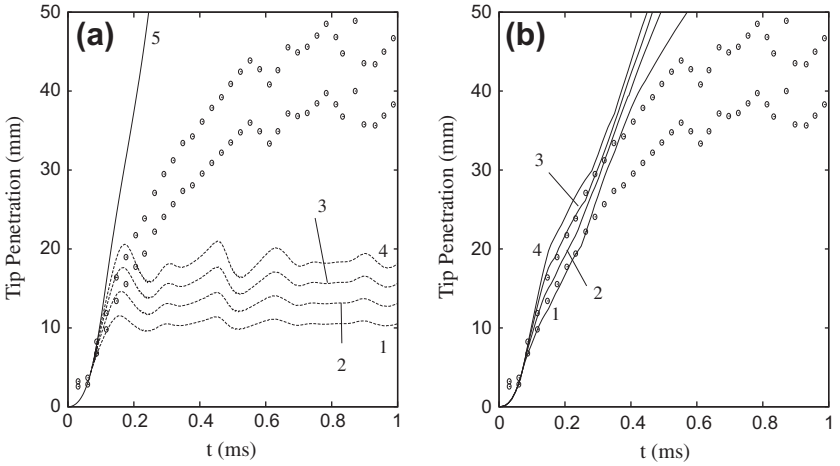

Fig. 8. Plot of (a) $L_s(t)$ (curve 5) and $L_{bu}(t)$ for the single hole injector with $B_1' = 2, 2.5, 3$ and 3.5 represented by curves 1–4 respectively. Panel (b) plots the penetration length of the spray predicted by the composite model with $B_1 = B_1'$ in the classic WAVE breakup model. The circles give the upper and lower limits of the error bars for the experimental observations.

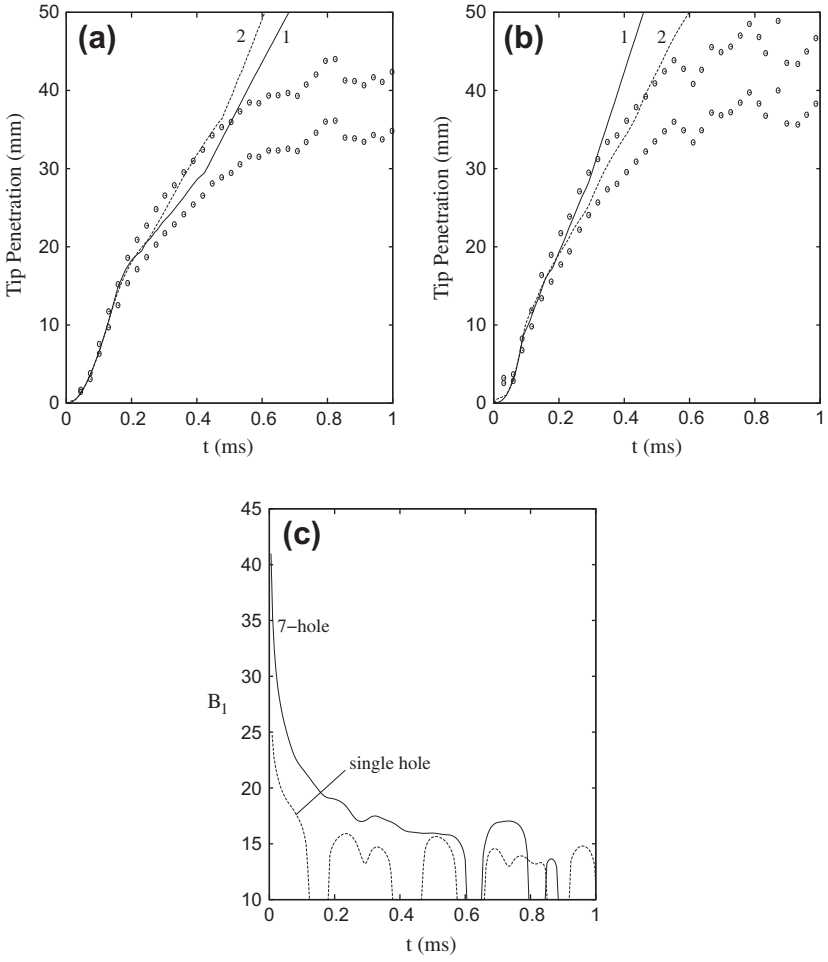

Fig. 9. Plot of the penetration length for both the composite model (curve 1) and the modified WAVE model (curve 2) for (a) the 7-hole injector and (b) the single hole injector. In panel (a) $B_1' = B_1 = 5$ for the composite model and $B_1 = 10$, $c_1 = 1$ and $c_2 = 0.2$ for the modified WAVE model, while in panel (b) $B_1' = B_1 = 2.5$ for the composite model and $B_1 = 10$, $c_1 = 0.5$ and $c_2 = 0.2$ for the modified WAVE model. Panel (c) plots the value of B_1^{mod} for each of the modified WAVE model results. The circles in (a) and (b) give the upper and lower limits of the error bars for the experimental observations.

factor of 3 or 4 times larger than the value of B_1, which would be the value of this constant in the steady jet case. This would correspond to an unsteady breakup time 3 or 4 times longer than the quasi-steady result from (3.2). However, the work of Turner et al. [35] does not support this four fold increase in the jet breakup time, which suggests that the composite model in this paper is more physically correct than the modified WAVE model.

Fig. 10 replots the composite WAVE model result for the 7-hole injector of Fig. 6b with $B_1' = 5$, along with composite model results using the TAB and stochastic breakup models. This figure shows that penetration length results, which are in good agreement with the experimental observations, can be generated via composite models using any of the classic spray breakup models in Sections 2.1,2.2,2.3. Here we find that all three results are practically indistinguishable from one another. This uniformity of the results is because we have removed the need for the unified droplet models to predict the primary breakup of the jet, and as such, the spray models here are only modelling the secondary breakup process. This agreement between the three models makes the inclusion of the jet breakup model even more convincing, and preferable to the modified WAVE model, because the secondary breakup can be described by any model without the need to damp the breakup process in these models.

The composite breakup model in its current form does need some improvements made, because the current shape of the spray does not agree well with the experimental data (see Fig. 17). This is because, although we have adjusted the total mass of fluid injected as droplets to take into account the mass of remaining fuel in the coherent core, we only release parcels of droplets with radius $r_d = r_s$ (calculated with $U_m = U_{\text{inj}}$ and $r_d = R$) from the end of the jet and with a velocity vector parallel to the axial direction of the jet. Therefore, there is no randomised droplet velocities at breakup, unlike in the classic breakup models. The correction for this issue is addressed in Section 7. However, another issue which needs to be addressed for both the jet breakup model and the WAVE spray model is the form of the velocity profile on which the linear stability analysis is performed. In the literature to date, the profile used is a plug flow jet shown in Fig. 1, and this profile has a velocity discontinuity at the fluid interface. However, in the actual experiments, the gas phase is viscous and so there exists a finite thickness shear layer in the gas phase. In Section 6 we examine the stability of such a profile, and investigate how it affects the results generated in Section 5.

6. Stability analysis of a liquid jet in a viscous gas phase

The velocity profile used in the stability analysis for the classic WAVE model assumes that the gas phase surrounding the jet is inviscid and therefore there is a discontinuity in velocity between the liquid and gas phases at the fluid interface, see Fig. 1 [63,64]. This velocity discontinuity means that, in the absence of viscosity,

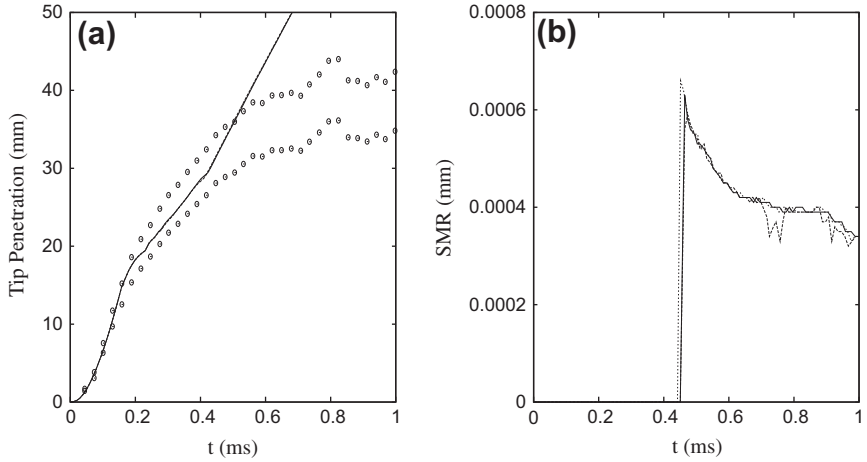

Fig. 10. Plot of (a) the penetration length and (b) the SMR, at $x = 30$ mm and $r = 0$ mm, for the composite breakup model with each of the three classic droplet breakup models WAVE (solid line), TAB (dashed line) and stochastic (dotted line) for modelling the secondary breakup process, with $B_1' = 5$ in the jet breakup model. This result is for the 7-hole injector with the results of all three models practically indistinguishable from one another in each panel. The circles give the upper and lower limits of the error bars for the experimental observations.

the growth rate properties of the instability waves generated by small disturbances in the jet, are determined solely by the surface tension of the liquid jet. This can be seen in expressions (2.3) and (2.4). However, in experiments the gas phase is viscous and so, due to the continuity of viscous stress at the fluid interface, there exists a finite thickness shear layer in the gas phase, as is schematically shown in Fig. 11. In this section we examine the stability properties of this type of velocity profile, and we show that the properties of the instability waves for this profile are not determined by the surface tension at large Weber numbers, but instead are determined by the thickness of the shear layer. This instability is known as the Rayleigh instability [65,66].

The major difference between the profile in Fig. 11, with a non-zero shear layer, and that in Fig. 1, is that no analytical dispersion relation can be derived, and therefore the stability properties, such as the form of Λ and Ω, have to be determined numerically. In this study we use a piecewise linear velocity profile with a linear profile in the shear layer, because we wish to determine whether or not the existence of such a shear layer is significant to the breakup properties. The approach suggested in this paper could also be used to investigate the stability properties of more realistic shear layer profiles, but we expect these results to be qualitatively similar to those produced in this paper. The piecewise linear profile in Fig. 11 has discontinuities in velocity gradient at $r = R$ and $r = (1 + \delta)R$, but the works of Esch [67] and Alabduljalil and Rangel [68] show that the properties of the fastest growing disturbance are very similar for both a piecewise linear profile and the smoothed version of the same profile.

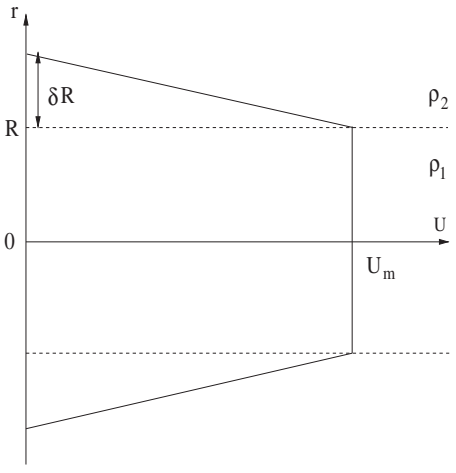

Fig. 11. Plot of the piecewise linear axial velocity profile $U(r)$ which incorporates a viscous gas phase outside of the jet, giving a continuous velocity profile at $r = R$. The thickness of the shear layer in the gas phase is δR.

To determine the stability equation for the velocity profile in Fig. 11 we first consider the Euler equations for an incompressible inviscid flow in cylindrical polar coordinates. The Euler equations are the usual Navier–Stokes equations with the viscous terms neglected. To determine whether or not the velocity profile in Fig. 11 is useful to the composite model, we consider an inviscid stability analysis, but viscous effects could be included by incorporating the viscous diffusion terms into the analysis below. Therefore, we do not explicitly consider the effect of viscosity in the breakup process, but we consider the effect of viscosity implicitly by the inclusion of the shear layer in the gas phase.

Assuming that the velocity components $(\tilde{u}, \tilde{v}, \tilde{w})$ are in the (x, θ, r) directions respectively, where x is the axial coordinate, the Euler equations take the form

$$\frac{1}{r}\frac{\partial(r\tilde{w})}{\partial r} + \frac{1}{r}\frac{\partial \tilde{v}}{\partial \theta} + \frac{\partial \tilde{u}}{\partial x} = 0, \tag{6.1}$$

$$\frac{\partial \tilde{w}}{\partial t} + \tilde{w}\frac{\partial \tilde{w}}{\partial r} + \frac{\tilde{v}}{r}\frac{\partial \tilde{w}}{\partial \theta} + \tilde{u}\frac{\partial \tilde{w}}{\partial x} - \frac{\tilde{v}^2}{r} = -\frac{1}{\rho}\frac{\partial \tilde{p}}{\partial r}, \tag{6.2}$$

$$\frac{\partial \tilde{v}}{\partial t} + \tilde{w}\frac{\partial \tilde{v}}{\partial r} + \frac{\tilde{v}}{r}\frac{\partial \tilde{v}}{\partial \theta} + \tilde{u}\frac{\partial \tilde{v}}{\partial x} - \frac{\tilde{w}\tilde{v}}{r} = -\frac{1}{\rho r}\frac{\partial \tilde{p}}{\partial \theta}, \tag{6.3}$$

$$\frac{\partial \tilde{u}}{\partial t} + \tilde{w}\frac{\partial \tilde{u}}{\partial r} + \frac{\tilde{v}}{r}\frac{\partial \tilde{u}}{\partial \theta} + \tilde{u}\frac{\partial \tilde{u}}{\partial x} = -\frac{1}{\rho}\frac{\partial \tilde{p}}{\partial x}. \tag{6.4}$$

We assume that the jet has a velocity vector which consists of a basic flow $(U(r), 0, 0)$, which only depends upon the radial coordinate, and a small perturbation which consists of disturbance waves with streamwise wavenumber α, azimuthal wavenumber n and angular frequency ω. Therefore, the velocity and pressure components take the form

$$\tilde{w}(r, x, t) = \epsilon w(r)\exp[i(\alpha x + n\theta - \omega t)], \tag{6.5}$$

$$\tilde{v}(r, x, t) = \epsilon v(r)\exp[i(\alpha x + n\theta - \omega t)], \tag{6.6}$$

$$\tilde{u}(r, x, t) = U(r) + \epsilon u(r)\exp[i(\alpha x + n\theta - \omega t)], \tag{6.7}$$

$$\tilde{p}(r, x, t) = P(r) + \epsilon p(r)\exp[i(\alpha x + n\theta - \omega t)], \tag{6.8}$$

where $\epsilon \ll 1$ and the lower case letters give the radial dependence of the perturbation.

These expressions are substituted into the Euler equations and linearised about ϵ. Therefore, retaining only terms of $O(\epsilon)$ we have

$$\frac{1}{r}\frac{\partial(rw)}{\partial r}+\frac{inv}{r}+i\alpha u=0, \tag{6.9}$$

$$-i\omega w+i\alpha Uw=-\frac{1}{\rho}\frac{\partial p}{\partial r}, \tag{6.10}$$

$$-i\omega v+i\alpha Uv=-\frac{inp}{\rho}, \tag{6.11}$$

$$-i\omega u+i\alpha Uu+\frac{dU}{dr}w=-\frac{i\alpha p}{\rho}. \tag{6.12}$$

As in [69–71], we focus our analysis in this section on axisymmetric disturbances ($n=0$), and neglect any contribution to the breakup process by non-axisymmetric disturbances. We make this assumption because we are considering the inviscid stability of the profile in Fig. 11, and [69,70] show that the disturbance wave with the largest growth rate is the axisymmetric mode, at large Weber numbers, in the inviscid and small viscosity cases respectively.

Eliminating u, v and p from the above four equations leads to the Rayleigh equation for w

$$(\alpha U-\omega)\left(\frac{d^2w}{dr^2}+\frac{1}{r}\frac{dw}{dr}-(1+\alpha^2r^2)\frac{w}{r^2}\right)+\alpha\left(\frac{1}{r}\frac{dU}{dr}-\frac{d^2U}{dr^2}\right)w=0. \tag{6.13}$$

This equation is solved for the temporal eigenvalue ω for a fixed value of α, where the eigenmode w satisfies the homogeneous boundary conditions

$$w(r=0)=0, \text{ and } w(r\to\infty)=0.$$

The velocity profile given in Fig. 11 can be split into three distinct regions given by

$$U(r)=\begin{cases}U_m & 0<r\leqslant R\\ U_m\left(1-\frac{r-R}{\delta R}\right) & R<r<R+\delta R,\\ 0 & R+\delta R<r\end{cases} \tag{6.14}$$

where U_m gives the jet velocity magnitude, and δ is the dimensionless thickness of the shear layer. The Rayleigh Eq. (6.13) is solved along with two supplementary equations which describe the continuity of both pressure and tangentional stress forces at the free surface, $r=R$. These equations are

$$\frac{w_1}{\alpha U_1-\omega}=\frac{w_2}{\alpha U_2-\omega}, \tag{6.15}$$

$$\rho_1(\alpha U_1-\omega)\left(\frac{dw_1}{dr}+\frac{w_1}{r}\right)-\rho_1\alpha\frac{dU_1}{dr}w_1-\rho_2(\alpha U_2-\omega)\left(\frac{dw_2}{dr}+\frac{w_2}{r}\right)+\rho_2\alpha\frac{dU_2}{dr}w_2=-\frac{\sigma\alpha^2(1-\alpha^2r^2)w_1}{r^2(\alpha U_1-\omega)}, \tag{6.16}$$

where σ is the surface tension and the subscripts 1 and 2 refer to the solutions in $0<r\leqslant R$ and $R<r<R(1+\delta)$ respectively. As we are using a piecewise linear velocity profile in this study, we also need to use the conditions (6.15) and (6.16) at $r=R(1+\delta)$ to jump over the discontinuity in the velocity gradient. However, as this discontinuity occurs in the same fluid phase, these equations are used with $\sigma=0$.

The Rayleigh Eq. (6.13) is solved for a complex ω for each real value of α using a shooting method technique [72]. We start by guessing an initial value for the eigenvalue ω for a given value of α, and begin integrating radially outwards from $r=0$. At this point we have the boundary condition $w=AI_1(\alpha r)$, and $dw/dr=A(\alpha I_0(\alpha r)-I_1/r)$, where I_0 and I_1 are modified Bessel functions of the first kind. These conditions are determined by solving (6.13) at small r, where $U=U_m$. We integrate (6.13) up to the fluid interface at $r=R$, where we use (6.15) and (6.16) to jump over the interface, by giving the change in w_2 and dw_2/dr across the interface, and we then continue integrating to large r values. In the large r limit we expect

$$w=BK_1(\alpha r),$$

where B is a constant and K_1 is the modified Bessel function of the second kind. We can now check if w behaves in this manner, else we update ω and repeat the integration process until w behaves in the correct manner. The value of ω is updated using Newton iterations by noting that

$$\frac{1}{w}\frac{dw}{dr}\sim-\alpha K_0(\alpha r)/K_1(\alpha r)-\frac{1}{r},$$

for large r.

In Fig. 12 we plot the stability analysis results for $\delta=0.025$, 0.05, 0.1, 0.2 and 0.3 numbered 1–5 in each panel. We plot these results for $We_1=10^5$, to give the case for large Weber numbers, but these results are identical for We_1 down to 10^3. As typical Weber number values for Diesel injections lie in the range $We_1\in[10^3,10^5]$, these results are valid for this entire range. Panel (a) plots the non–dimensional wavenumber $R\delta\alpha_m$ of the fastest growing wave as a function of q. We choose to plot the quantity $R\delta\alpha_m$ because for these values of δ the results almost collapse onto one single result for $q\in[1/100,1/10]$. For a single planar shear layer, where the only length scale is the shear layer thickness, Marmottant and Villermaux [66] showed that the results for $\hat{\delta}\alpha_m$ were solely a function of the quantity $\hat{\delta}We_2$, i.e. independent of $\hat{\delta}$, where $\hat{\delta}$ is the dimensional shear layer thickness. The problem here, however, is more complicated because we have a second length scale in the problem, that of the jet radius, so the results do not collapse exactly onto one single result. However, the results do collapse quite well in the range of q values that we are interested in ($q\in[1/100,1/10]$), and in fact in this region $R\delta\alpha_m\approx1.1q^{0.45}$, which is the estimate given by the solid line. The result for the maximum growth rate $R\delta\Omega/U_m$ in panel (b) however, is more sensitive to having two length scales in the problem, but we still find a reasonable collapse of the results for $q\in[1/100,1/10]$. As the value of δ increases this agreement becomes less visible as can be seen for the $\delta=0.2$ and 0.3 results. However, as we have no experimental results to determine an exact value for δ, we make the approximation for the results in panel (b) of $R\delta\Omega/U_m\approx0.55q^{0.95}$ (solid line) so that we can illustrate the effect of a viscous gas phase in the composite breakup model. The thickness of the shear layer is also likely to vary for different injection pressures and different nozzle types. The results of Turner et al. [35,73] show that $\delta\in[0.1,0.3]$ by using CFD simulations to model the Diesel injection process. Panel (c) shows that there is no way to easily collapse the value of the group velocity of the wave packet onto one solution, so we just note that in the range $q\in[1/100,1/10]$ the group velocity $c_g/U_m\in[0.7,0.95]$. The effect of this group velocity, being lower than the group velocity of the Kelvin–Helmholtz problem, on the model will be discussed in Section 7.

In Fig. 13 we plot (a) $R\omega_i/U_m(R\alpha)$ and (b) $R\alpha_m(We_2)$ for $\delta=0.1$ and $q=1/50$ showing the transition from the zero thickness shear layer Kelvin–Helmholtz instability to the finite thickness shear layer Rayleigh instability. Panel (a) shows the non–dimensional growth rate curve which is initially dominated by a peak around $R\alpha=0.5$ but as We_2 is increased, i.e. the influence of the shear layer is increased, a second peak appears around $R\alpha=2$ and rapidly increases in magnitude over a very short range of We_2 values. This

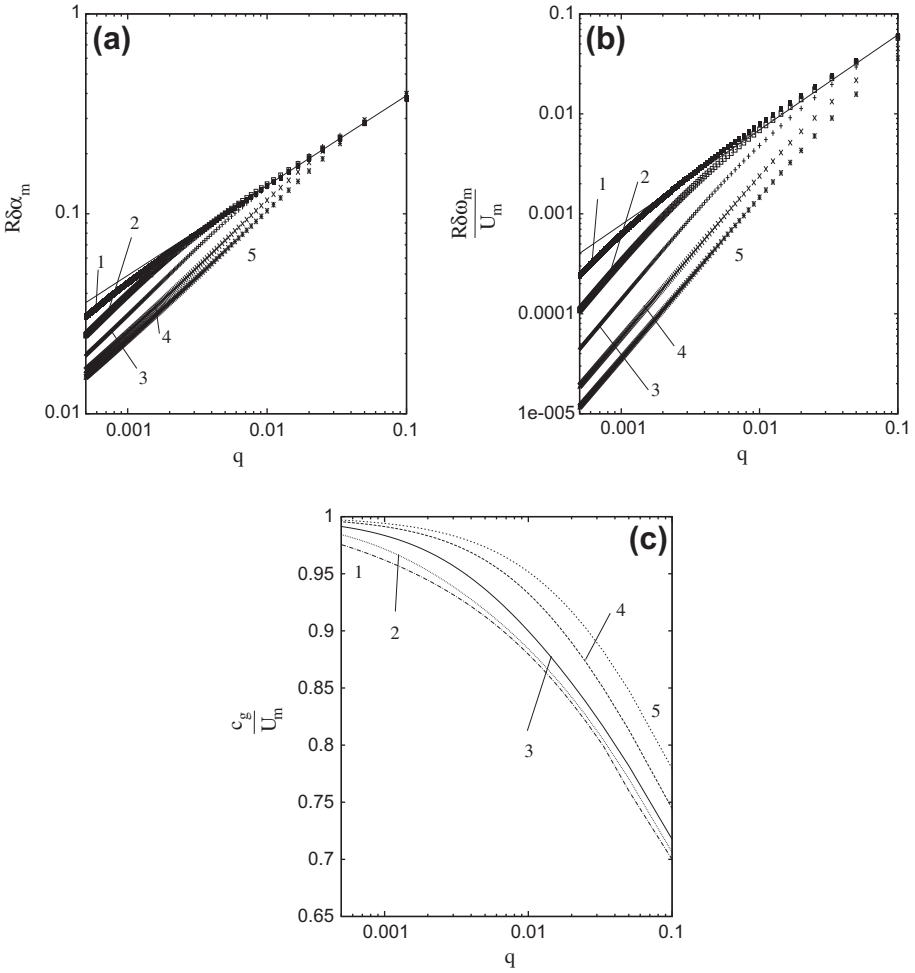

Fig. 12. Plot of (a) the non–dimensional wavenumber $R\delta\alpha_m$ of the fastest growing wave, (b) the maximum growth rate $R\delta\Omega/U_m$ at $R\alpha = R\alpha_m$ and (c) the wave speed c_g/U_m at $R\alpha = R\alpha_m$, all as a function of q, for $We_1 = 10^5$. In each panel the results are plotted for $\delta = 0.025$, 0.05, 0.1, 0.2 and 0.3, numbered 1–5 respectively, and the solid lines in panels (a) and (b) are the approximations $R\delta\alpha_m \approx 1.1q^{0.45}$ and $R\delta\Omega/U_m \approx 0.55q^{0.95}$ respectively.

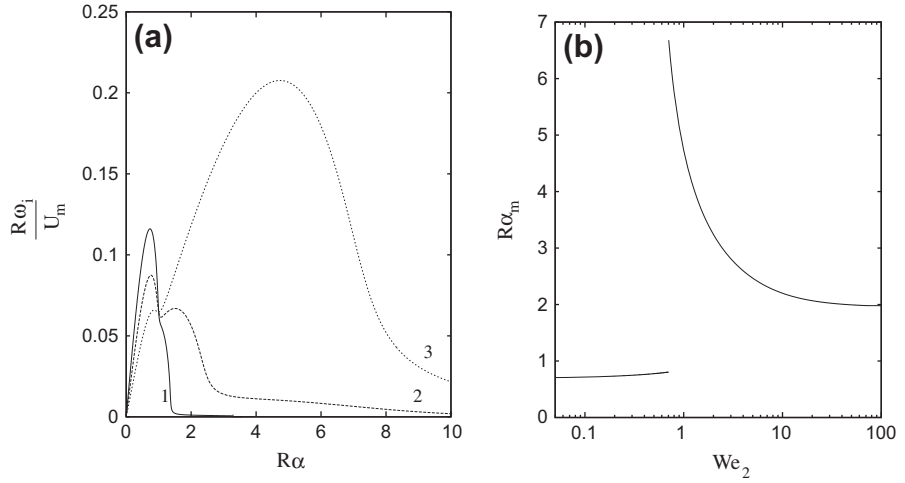

Fig. 13. Plot of (a) $R\omega_i/U_m(R_\alpha)$ for $We_2 = 0.2$, 0.4 and 1 numbered 1–3 respectively and (b) $R\alpha_m(We_2)$ for $\delta = 0.1$ and $q = 1/50$. This figure shows the transition from the Kelvin–Helmholtz instability to the Rayleigh instability as We_2, and hence the influence of the shear layer, increases.

is illustrated in panel (b) which shows the rapid transition of the value of $R\alpha_m$. For these values of δ and q the transition occurs around $We_2 = 1$, and for Diesel jet injections $We_2 = We_1 q \in$ [20, 2000] so we can clearly see that we are in the regime where the thickness of the shear layer is significant to the stability characteristics of the jet. Thus using the stability results (2.3) and (2.4)

is not the correct approach for this case. We propose the following alternative approximation for these values from the best fit lines in Fig. 12:

$$\Lambda \approx 5.71 q^{-0.45} \delta R, \tag{6.17}$$

$$\Omega \approx \frac{0.55 q^{0.95} U_m}{\delta R}, \tag{6.18}$$

for $q \in [1/100, 1/10]$ and for values of $\delta \in [0.025, 0.3]$.

These new results can be incorporated into the WAVE model in the droplet stripping regime by defining the new break up time and stable droplet radius as

$$\tau_{\text{bu}} = 3.141 \frac{B_1 R}{\Lambda \Omega}, \tag{6.19}$$

$$r_s = \frac{0.39 \Lambda}{\text{We}_1^{0.45} \delta}. \tag{6.20}$$

These variables are determined using the same conditions as were used to derive (2.5) and (2.2). Notably, the constant 3.141 in (6.19) is found such that (6.19) reduces to (3.2) for high speed flows, and (6.20) is determined using the threshold for bag breakup $\text{We}_2 = 6$ [19], and rearranging (6.17) to solve for $R \equiv r_s$, noting that $q = \text{We}_2/\text{We}_1$. By examining the forms of r_s in the large We_1 limit, from the first equation of (2.2) (with $Z = T = 0$) and (6.20), we find

$$r_s^{\text{KH}} = \frac{5.98 R}{\text{We}_2},$$

$$r_s^{\text{R}} = \frac{2.23 R}{\text{We}_2^{0.45}},$$

which shows that the droplets formed at breakup by the Rayleigh instability are larger than those of the Kelvin–Helmholtz instability. This fact turns out to be significant for the results in the next section.

The form of (6.17) and (6.18), which have been chosen to approximate the linear stability data, means that the results in Section 7 are independent of the value of δ, as can be seen above. But for the values of q we are interested in, we expect the small deviations from these approximations in Fig. 12 to only make a small difference to our results. The reason for making the approximations we did in (6.17) and (6.18) is to allow this new profile to be easily incorporated into existing spray and jet breakup models without the need to re-solve the Rayleigh equation. This will benefit those who wish to incorporate this velocity profile into these breakup models, and have little experience of solving the Rayleigh equation.

7. Results of the composite spray breakup model with a viscous gas phase

In this section we examine results for the composite breakup model which uses the stability theory of the piecewise linear velocity profile with the viscous gas phase from Section 6. We also examine the shape of the sprays to see whether or not the shapes predicted by the viscous gas model agree with experimental observations. However, before we investigate the composite model, we briefly investigate how the new model parameters (6.17) and (6.18) modify the results of the classic WAVE model in Fig. 14. These results show that the viscous gas velocity profile with the shear layer in the gas phase makes no significant difference to the penetration result for the classic WAVE model. However, panel (b) shows that the radius of the droplets produced by the stripping process are increased by approximately 25% on average. The significance of this is seen later in this section.

In Fig. 15a we plot the penetration length of the spray for the single hole injector, comparing the composite model incorporating both the WAVE breakup model with the inviscid gas phase profile and the WAVE model with the viscous gas phase profile and the classic WAVE model, which has no coherent jet, with $B_1' = B_1 = 2.5$. These results show that the two composite models give very similar penetration lengths and both these differ greatly from the classic WAVE model. Fig. 15b shows the SMR at $x = 30$ mm and $r = 0$ mm for the three models, and the solid circles give experimental data points of the average SMR taken in the vicinity of this point [74]. It is clear from panel (a) that the two composite model results are going to agree better with the first data point than the classic model because the penetration length is well predicted by these composite models. The two composite model results are also in good agreement with the experimental data points for $t > 0.3$ ms, which shows that this composite model produces correct droplet sizes in the spray. As both composite models produce a similar level of agreement with the experimental points, it appears that the modification of the WAVE model in Section 6 is not required. However, when we look at the shape of the generated spray and the droplet size distribution in the spray, we see that this modification does make a difference.

Fig. 16 shows an image of one of the sprays from the experiment for the 7-hole injector taken at 0.5 ms after injection. It shows that the spray near the nozzle has a conical shape, where droplets are expected to be stripped off the side of the coherent core, but the main part of the core is masked by the droplets (as found in the experiments of Yule and Filipovic [38]). This figure

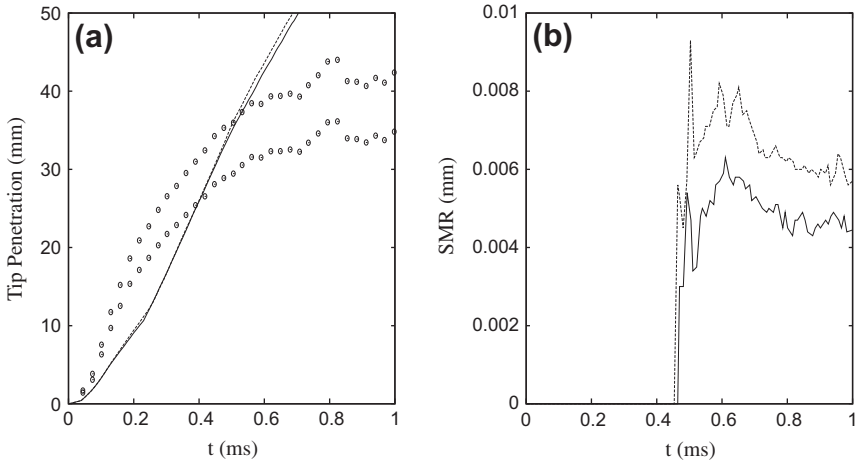

Fig. 14. Plot of the classic WAVE model result with $B_1 = 10$ from Fig. 4 (solid curve) and the corresponding result for the velocity profile with a finite thickness shear layer in the gas phase (dashed curve) for (a) the penetration length and (b) the SMR at $x = 30$ mm and $r = 0$ mm.

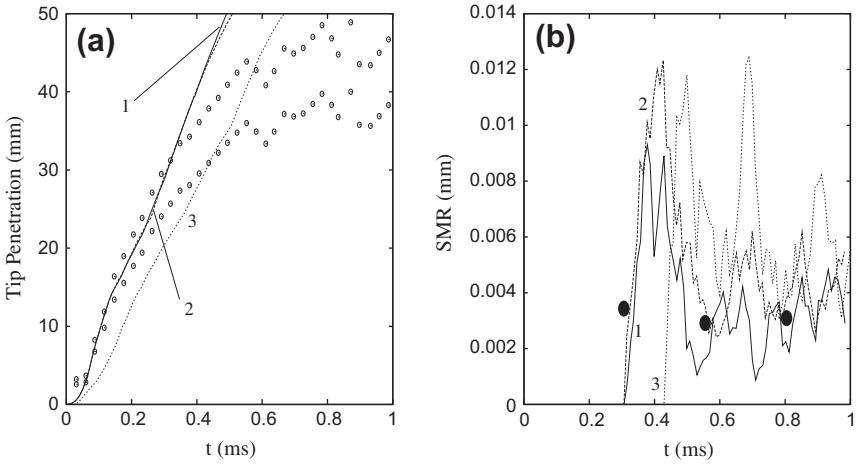

Fig. 15. Comparison for the single hole nozzle experiment of the composite model incorporating the WAVE model with an inviscid gas phase velocity profile (result 1), the composite model incorporating the WAVE model with a viscous gas phase velocity profile (result 2) and the classic WAVE model result (result 3) each with $B_1' = B_1 = 2.5$ for (a) the penetration length and (b) the SMR at $x = 30$ mm and $r = 0$ mm. The SMR results are averaged over 4 data points to smooth the results and make them more informative. The experimental data points in (b) come from [74].

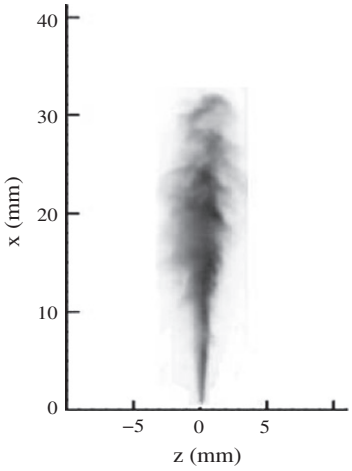

Fig. 16. Photo of a spray from the experiment for the 7-hole injector with $p_{inj} = 60$ MPa and $p_g = 2$ MPa at 0.5 ms after injection.

shows a very dense central region of droplets for $x \lesssim 23$ mm which we expect to behave as an intact liquid core (cf. the experimental results of Sakaguchi et al. [36]). When we examine the spray shape from the different breakup models in Fig. 17 we see similarities between these results and the experimental result in Fig. 16.

The spray shape results in Fig. 17 show that the classic WAVE model (panel (a)) gives a good overall spray shape but with a poor penetration length prediction at early times (see Fig. 4a). This classic model also has a string of droplets for $x < 10$ mm, which approximate the coherent liquid core, which decreases in radius before thickening out at the point of primary breakup. However, the experimental result in Fig. 16 shows a dense spray region which has a radius that increases slightly for $x < 10$ mm. The composite WAVE model result with the inviscid velocity profile (panel (b)) gives a good penetration length prediction for $t < 0.5$ ms but a poor spray shape. This is due to the missing random droplet velocity direction at primary breakup which the classic WAVE model has included in its formulation. In panels (c) and (d) we consider the composite WAVE model with the instability data from the inviscid gas phase velocity profile and the viscous gas phase velocity profile respectively. For these two results we have randomised our droplet velocities by introducing a cone angle of 20° in which the droplets can leave both the end and the side of the jet. This value was used because it was measured in the experiments of Karimi [52] for this injection nozzle. We have also allowed the injected droplets, at each time value, to be randomly released from the side of the jet, and not just from the tip, in the range $[0.25, 1] \times L_{bu}$. This is possible without violating mass conservation, because we are still stripping the same, N say, droplets from the core, but they are now allowed to leave the side of the core as well as from the tip. However, at this stage we still allow the core to remain cylindrical. This approach is taken because experiments, such as those of Yule and Filipovic [38], show an intact column of fluid surrounded by droplets which have been stripped off the side of the column. In this study we use the value of 0.25 but this will depend upon the type of injector used, and possibly on the values of p_{inj} and p_g. This value is chosen because the observed spray shown in Fig. 16 appears to have a region for $x \lesssim 10$ mm where the main part of the spray remains approximately cylindrical, before spreading out for $x \gtrsim 10$ mm where there is a dense region of droplets, and this value also gives results which agree with this behaviour (Fig. 17c and d).

In panels (c) and (d) we note that the predicted shape of the sprays is closer to the observed one for the case where the viscous gas phase is considered. This is because this model produces droplets with larger radii as they are stripped off the coherent jet. These larger droplets have greater momentum than the smaller droplets in panel (c), and hence are distributed wider into the gas phase. If we were also to include viscosity explicitly into our breakup mechanism then the droplets would be larger still, allowing them to penetrate further into the gas phase which is likely to give a shape which agrees better with that of the experimental spray in Fig. 16. The effect of viscosity, however, is not considered in this paper as we are focused on understanding how to generate more accurate penetration length results whilst still predicting droplet distributions and spray shapes which give reasonable agreement with experiments. By introducing the cone angle to the simulation we slightly reduce the penetration length of the spray, which can be seen in Fig. 18a, but the results still fall within the error bars of the experimental data up to $t \approx 0.6$ ms. Fig. 18b shows the droplet size distribution function, $f(r_d) = F(r_d)/N$, for 0.1 μm intervals found in the spray, where $F(r_d)$ is the droplet number distribution defined in Section 2.3 and N is the total number of droplets. This figure shows that the two spray results in Fig. 17b and c, which both use the inviscid velocity profile, contain smaller droplets on

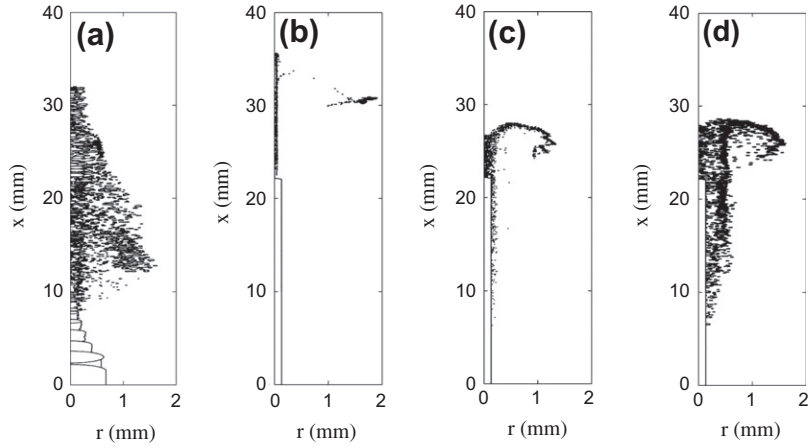

Fig. 17. Plot of the spray shapes for the 7-hole injector at $t = 0.5$ ms for (a) the classic spray model, (b) the composite model with the inviscid gas phase profile and zero spray angle, (c) the composite model with the inviscid gas phase profile and 20° spray angle and (d) the composite model with the viscous gas phase profile and 20° spray angle, all with $B_1 = B_1' = 5$. In panel (a) all the droplets are 10 times actual size, in panels (b) and (c) the droplets are 20 times actual size, the jet is 2 times actual size and in panel (d) the droplets are 10 times actual size, and the jet is 2 times actual size. See Fig. 18b for droplet sizes.

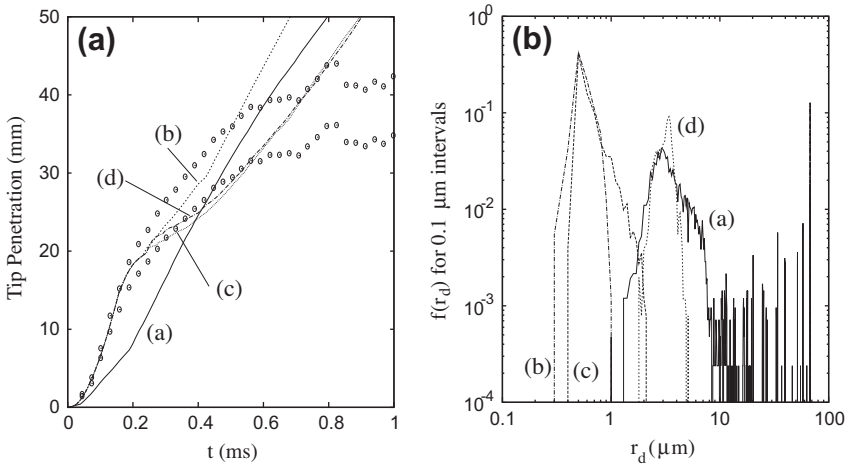

Fig. 18. Plot of (a) the penetration lengths for the results plotted in Fig. 17 and (b) the size distribution, $f(r_d)$, of droplets for 0.1 μm intervals about r_d. The labels correspond to the individual panel labels.

average compared to the classic WAVE model and the viscous gas phase velocity profile model. The classic WAVE and viscous gas phase models both contain a peak droplet radius of approximately 3 μm. The classic WAVE model obviously contains regions of larger droplets due to the way primary breakup is implemented through (2.1), but the range of most frequent droplet sizes is very similar to the composite model.

From Fig. 12c we observe that the value of c_g/U_m for Diesel jets with a finite thickness shear layer is usually less than *1*, whereas we have assumed it to be exactly 1 so far in this paper. However, considering a more realistic value of c_g/U_m does not affect the results presented in this paper, as we see in Figs. 19 and 20. In these figures we consider the 7-hole injector experiment and assume that $\delta = 0.1$, and thus $c_g/U_m = 0.81$ from Fig. 12c for $q = 0.0227$. In Fig. 19a we see that this value of c_g/U_m means that the L_{bu} curves no longer join onto the L_s curve, and there is a discontinuity in the breakup length at this point. In Fig. 19b we observe what effect this has on the penetration lengths generated using the KIVA II code. We find that the calculated penetration length is reduced slightly from the $c_g/U_m = 1$ result, because the breakup lengths themselves are slightly reduced, and the discontinuity in L_s and L_{bu} can be seen in Fig. 19a between 0.1 ms $\leqslant t \leqslant$ 0.2 ms. The reduction in the breakup length can be overcome by increasing the model constant $B_1' = B_1$, where we now find that $B_1' = B_1 = 7$ gives better results rather than $B_1' = B_1 = 5$, but $B_1' = B_1 = 7$ still lies within the range of acceptable values discussed earlier.

We can eliminate the discontinuity between L_s and L_{bu} by relaxing our assumption that the velocity throughout the core, in particular at the tip of the core, is constant and equal to U_{inj}. This approach is more realistic and is supported by the experiments of Sakaguchi et al. [36], who find a slow decrease in the velocity within the core in the streamwise direction, i.e. the tip velocity is less than the injection velocity. A similar example of this streamwise velocity variation can be seen for a planar jet in Söderberg and Alfredsson [75]. Here we aim for qualitative agreement with the behaviour seen in [36], so we assume that

$$U_m^{tip} = U_{inj}(1 - U't), \tag{7.1}$$

where U' is a constant which is adjusted to ensure that L_s (curve 3) meets the curve L_{bu} (curve 2) as shown in Fig. 20a. This occurs for $U' \approx 1625\ s^{-1}$. This is solely an aesthetic change to the penetration length we calculate, as we have not assumed that any droplet parcels have been released from the jet before this time, as we are in

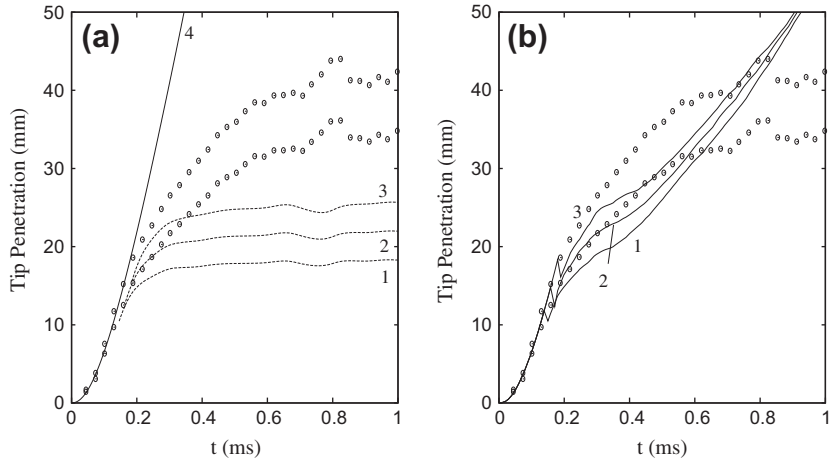

Fig. 19. Plot of (a) $L_s(t)$ (curve 4) and $L_{bu}(t)$ for the 7-hole injector with $B_1' = 5, 6$ and 7 represented by curves 1–3 respectively with $c_g/U_m = 0.81$ in the jet breakup model. Panel (b) plots the penetration length of the composite model with $B_1 = B_1'$ in the WAVE breakup model.

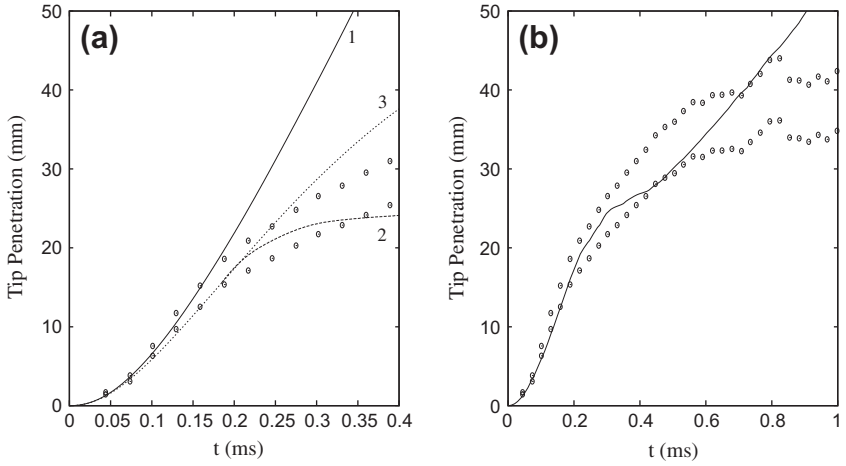

Fig. 20. Plot of (a) $L_s(t)$ (curve 1) and $L_{bu}(t)$ (curve 2) for the 7-hole injector with $B_1' = 7$ and $c_g/U_m = 0.81$. Curve 3 in panel (a) plots $L_s(t)$ where the tip velocity of the jet has been linearly modified using (7.1) to match onto the initial value of $L_{bu}(t)$. Panel (b) plots the penetration length of the composite model with $B_1 = B_1'$ in the WAVE breakup model with the modified value of $L_s(t)$ using (7.1) so that it joins onto the jet breakup length L_{bu}.

the region $t < \tau_b(t_0)$. The resulting penetration length can be seen in Fig. 20b. In theory one could then adjust the velocities (and thus the size) of the droplets leaving the core, but this would require a spatio-temporal evolution of the core, which is not available at this time. All the sprays shown in Figs. 19 and 20 have shapes and size distributions very similar to that in Fig. 17d, so this different value of c_g/U_m does not affect the spray characteristics.

8. Conclusions

This paper describes a composite breakup model for the analysis of transient sprays, such as those found in Diesel engines. The core of the spray, consisting of a jet, ligaments and densely packed droplets, was modelled as a coherent liquid jet which undergoes primary breakup. The characteristic breakup time and length of the core were defined using linear stability analysis of a liquid jet. This model was composed with the classic WAVE breakup model and incorporated into the CFD package KIVA II to produce spray penetration results which agreed well with the experimental observations for transient Diesel fuel sprays [52]. In comparison with the spray breakup model of Sazhin et al. [6], who incorporated the effect of the coherent liquid core, the present model does not require empirical parameters to control the viscous damping of the Kelvin–Helmholtz instability due to jet acceleration, to obtain agreement with experiments.

We also investigated the linear stability of a velocity profile which incorporated a finite thickness shear layer in the gas phase, which is more realistic than the plug flow profile assumed in the derivation of previous models of jet breakup [19,63]. The inclusion of the viscous velocity profile predicted that larger droplets are stripped from the core at primary breakup in the large Weber number stripping regime compared to the inviscid velocity profile. This gave spray shapes which agreed better with the experimental observations.

Acknowledgment

This work is supported by the EPSRC under Grants EP/F069855/1 and EP/G000034/1.

References

[1] Flynn PF, Durrett RP, Hunter GL, zur Loye AO, Akinyemi OC, Dec JE, et al. Diesel combustion: an integrated view combining laser diagnostics chemical kinetics and empirical validation. SAE Paper 1999-01-0509; 1999.
[2] Bertoli C, na Migliaccio M. A finite conductivity model for diesel spray evaporation computations. Int J Heat Fluid Flow 1999;20:552–61.

[3] Sazhina EM, Sazhin SS, Heikal MR, Babushok VI, Johns R. A detailed modelling of the spray ignition process in diesel engines. Combust Sci Technol 2000;160:317–44.
[4] Zhou P, Zhou S, Clelland D. A modified quasi-dimensional multi-zone combustion model for direct injection diesels. Int J Engine Res 2006;7(4): 335–45.
[5] Wang Y, Rutland CJ. Direct numerical simulation of ignition in turbulent n-heptane liquid-fuel spray jets. Combust flame 2007;149(4):353–65.
[6] Sazhin SS, Martynov SB, Kristyadi T, Crua C, Heikal MR. Diesel fuel spray penetration, heating, evaporation and ignition: modelling vs. experimentation. Int J Eng Syst Modell Simul 2008;1(1):1–19.
[7] Amsden AA, O'Rourke PJ, Butler TD. KIVA II: a computer program for chemically reactive flows with sprays. Los-Alamos National Laboratory Report No. LA–11560-MS; 1989.
[8] Reitz RD, Rutland CJ. Development and testing of diesel engine CFD models. Prog Energy Combust Sci 1995;21:173–96.
[9] Gosman AD, Clerides D. Diesel spray modelling: a review. In: Proceedings of ILASS-Europe, Florence, Italy; 1997.
[10] Stiesch G. Modelling engine sprays and combustion processes. Berlin: Springer; 2003.
[11] Yi Y, Reitz RD. Modelling the primary breakup of high-speed jets. Atomiz Sprays 2004;14:53–80.
[12] Nijdam JJ, Guo B, Fletcher DF, Langrish TAG. Lagrangian and Eularian models for simulating turbulent dispersion and coalescence of droplets within a spray. Appl Math Modell 2006;30:1196–211.
[13] Kim S, Lee CS. Improvement of the grid dependency of the momentum coupling and the droplet collision modeling in the arbitrary Lagrangian–Eulerian method for spray simulations. In: Proc ICLASS-2009, Colorado, USA; 2009.
[14] Sazhin SS, Kristyadi T, Abdelghaffar WA, Heikal MR. Models for fuel droplet heating and evaporation: comparative analysis. Fuel 2006;85:1613–30.
[15] Faeth GM, Hsiang L-P, Wu P-K. Structure and breakup properties of sprays. Int J Multiphase Flow 1995;21:99–127.
[16] Chryssakis C, Assanis DN. A unified fuel spray breakup model for internal combustion engine applications. Atomiz Sprays 2008;18:1–52.
[17] Reitz RD, Diwakar R. Structure of high-pressure fuel sprays. SAE Paper 870598; 1987.
[18] O'Rourke PJ, Amsden AA., The Tab method for numerical calculation of spray droplet breakup. SAE Paper 872089; 1987.
[19] Reitz RD. Modelling atomization processes in high-pressure vaporizing sprays. Atomiz Spray Technol 1987;3:309–37.
[20] Patterson MA, Reitz RD. Modelling the effects of fuel spray characteristics on diesel engine combustion and emission. SAE Paper 980131; 1998.
[21] Beale JC, Reitz RD. Modelling spray atomization with the Kelvin–Helmholtz/Rayleigh–Taylor hybrid model. Atomiz Sprays 1999;9:623–50.
[22] Kong SC, Senecal PK, Reitz RD. Developments in spray modelling in diesel and direct-injection gasoline engines. Oil Gas Sci Technol Rev IFP 1999;54(2): 197–204.
[23] Gorokhovski MA, Saveliev VL. Analysis of Kolmogorov's model of breakup and its application into Lagrangian computation of liquid sprays under air-blast atomisation. Phys Fluids 2003;15(1):184–92.
[24] Kolmogorov AN. On the log–normal distribution of particle sizes during the breakup process. Dokl Akad Nauk SSSR 1941;31:99.
[25] Rimbert N, Séro-Guillaume O. Log-stable laws as asymptotic solutions to a fragmentation equation: application to the distribution of droplets in a high Weber-number spray. Phys Rev E 2004;69:056316.
[26] Gorokhovski M, Jouanguy J, Chtab A. LES with stochastic simulation of primary and secondary air-blast atomization. In: Proc ICLASS-2006, Kyoto, Japan; 2006.
[27] Gorokhovski M, Saveliev VL. Statistical universalities in fragmentation under scaling symmetry with a constant frequency of fragmentation. J Phys D: Appl Phys 2008;41:085405.
[28] Gorokhovski M, Jouanguy J, Chtab-Desportes A. Stochastic model of the near-to-injector spray formation assisted by a high-speed coaxial gas jet. Fluid Dyn Res 2008;41(3):035509.
[29] Gorokhovski M, Herrmann M. Modeling primary atomization. Annu Rev Fluid Mech 2008;40:343–66.
[30] Pozorski J, Sazhin S, Waclawczyk M, Crua C, Kennaird D, Heikal M. Spray penetration in a turbulent flow. Flow Turbul Combust 2002;68:153–65.
[31] Sazhin SS, Feng G, Heikal M. A model for fuel spray penetration. Fuel 2001;80:2171–80.
[32] Sazhin SS, Crua C, Kennaird D, Heikal M. The initial stage of fuel spray penetration. Fuel 2003;82:875–85.
[33] Sarre CK, Kong S-C, Reitz RD. Modelling of the effects of injector nozzle geometry on diesel sprays. SAE Paper 1999-01-0912; 1999.
[34] Kaario O, Larmi M, Tanner FX. Non-evaporating liquid spray simulations with the ETAB and WAVE droplet breakup models. In: Proceedings of ILASS-Europe, Zaragoza, Spain; 2002.
[35] Turner MR, Healey JJ, Sazhin SS, Piazzesi R. Wave packet analysis and break-up length calculations for accelerating planar liquid jets. Fluid Dyn Res 2012;44:015503.
[36] Sakaguchi D, Yamamoto S, Ueki H, Ishdia M. Study of heterogeneous structure in diesel fuel spray by using micro-probe L2F. J Fluid Sci Technol 2010;5(1): 75–85.
[37] Crua C, Shoba T, Heikal M, Gold M, Higham C. High-speed microscopic imaging of the initial stage of diesel spray formation and primary breakup. SAE Paper 2010-01-2247; 2010.
[38] Yule AJ, Filipovic I. On the break-up times and lengths of diesel sprays. Int J Heat Fluid Flow 1992;13(2):197–206.
[39] Badock C, Wirth R, Fath A, Leipertz A. Investigation of cavitation in real size diesel injection nozzles. Int J Heat Fluid Flow 1999;20:538–44.
[40] Smallwood GJ, Gülder OL, Snelling DR. The structure of the dense core region in transient diesel sprays. In: Twenty-fifth international symposium on combustion. The Combustion Institute; 1994. p. 371–9.
[41] Lin SP, Reitz RD. Drop and spray formation from a liquid jet. Annu Rev Fluid Mech 1998;30:85–105.
[42] Reinecke WG, Waldman GD. A study of drop breakup behind strong shocks with applications to flight. AVCO Report AVSD–0110-70-RR, May 1970.
[43] Hiroyasu H, Kadota T. Fuel droplet size distribution in a diesel combustion chamber. SAE Paper 740715; 1974.
[44] Tanner FX. Development and validation of a cascade atomization and drop breakup model for high-velocity dense sprays. Atomiz Sprays 2004;14: 211–42.
[45] Narasimha R, Sreenivasan KR. Relaminarization of fluid flows. Adv Appl Mech 1979;19:221–301.
[46] Lozano A, Barreras F, Hauke G, Dopazo C. Longitudinal instabilities in an air-blasted liquid sheet. J Fluid Mech 2001;437:143–73.
[47] Cebeci T. SAMO analysis of turbulent boundary layers series: applied mathematics and mechanics. New York: Academic Press; 1974.
[48] Nordin N. Complex chemistry modeling of diesel spray combustion. PhD thesis. Gothenburg (Sweden): Chalmers University of Technology; 2001.
[49] O'Rourke PJ. Collective drop effects on vaporizing liquid sprays. PhD thesis. Princeton (USA): Princeton University; 1981.
[50] Karimi K, Sazhina EM, Abdelghafffar WA, Crua C, Heikal MR, Gold MR. Development in diesel spray characterisation and modelling. In: Proceedings of THIESEL-2006 Valencia, Spain; 2006.
[51] Abdelghaffar WA, Elwardany AE, Sazhin SS. Modeling of the processes in diesel engine-like conditions: effects of fuel heating and evaporation. Atomiz Sprays 2010;20(8):737–47.
[52] Karimi K. Characterisation of multiple-injection diesel sprays at elevated pressures and temperatures. PhD thesis. Brighton (United Kingdom): University of Brighton 2007.
[53] Schugger C, Meingast U, Renz U. Time-resolved velocity measurments in the primary breakup zone of a high pressure diesel injection nozzle. In: Proceedings of ILASS-Europe, Darmstadt, Germany; 2000.
[54] Juniper MP. The full impulse response of two-dimensional jet/wake flows and implications for confinement. J Fluid Mech 2007;590:163–85.
[55] Juniper MP. The effect of confinement on the stability of non-swirling round jet/wake flows. J Fluid Mech 2008;605:227–52.
[56] Nicholls J. Stream and droplet breakup by shock waves. In: Harrje DT, Reardon FH, editors. NASA SP-194 liquid propellant rocket combustion instability; 1972. p. 126–8.
[57] Crua C. Combustion processes in a diesel engine. PhD thesis. Brighton (United Kingdom): University of Brighton; 2002.
[58] Arcoumanis C, Gavaises M, French B. Effect of fuel injection processes on the structure of diesel sprays. SAE Paper 970799; 1997.
[59] Nurick WH. Orifice cavitation and its effect on spray mixing. J Fluid Eng 1976;98:681–7.
[60] Tonini S, Gavaises M, Theodorakakos. Modelling of high-pressure dense diesel sprays with adaptive local grid refinement. Int J Heat Fluid Flow 2008;29:427–48.
[61] Levich VG. Physiochemical hydrodynamics. Englewood Cliffs (NJ): Prentice-Hall; 1962.
[62] Desantes JM, Payri R, Salvador FJ, Gimeno J. Measurements of spray momentum for the study of cavitation in diesel injection nozzles. SAE Paper 2003-01-0703; 2003.
[63] Reitz RD, Bracco FV. Mechanisms of breakup of round liquid jets. In: Encyclopedia of fluid mechanics. Gulf Pub.; 1986.
[64] Reitz RD, Bracco FV. Mechanism of atomization of a liquid jet. Phys Fluids 1982;25(10):1730–42.
[65] Rayleigh Lord. The theory of sound. 2nd ed. London: Macmillian; 1894.
[66] Marmottant P, Villermaux E. On spray formation. J Fluid Mech 2004;498:73–111.
[67] Esch RE. The instability of a shear layer between two parallel streams. J Fluid Mech 1957;3:289–303.
[68] Alabduljalil S, Rangel RH. Inviscid instability of an unbounded shear layer: effect of surface tension, density and velocity profile. J Eng Math 2006;54: 99–118.
[69] Yang HQ. Asymmetric instability of a liquid jet. Phys Fluids 1991;4(4):681–9.
[70] Li X. Mechanism of atomization of a liquid jet. Atomiz Sprays 1995;5: 89–105.
[71] Ruo A-C, Chang M-H, Chen F. On the nonaxisymmetric instability of round liquid jets. Phys Fluids 2008;20(6):062105.
[72] Stoer J, Bulirsch R. Introduction to numerical analysis. New York: Springer; 1980.
[73] Turner MR, Healey JJ, Sazhin SS, Piazzesi R. Stability analysis and break-up length calculations for steady planar liquid jets. J Fluid Mech 2011;668: 384–411.
[74] Lacoste J. Characteristics of diesel sprays at high temperatures and pressures. PhD thesis. Brighton (United Kingdom): University of Brighton; 2005.
[75] Söderberg LD, Alfredsson PH. Experimental and theoretical stability investigations of plane liquid jets. Eur J Mech B: Fluids 1998;17: 689–737.